Neurobiology of Disease 62 (2014) 441–455

Contents lists available at ScienceDirect

Neurobiology of Disease

journal homepage: www.elsevier.com/locate/ynbdi

Galectin-3 controls the response of microglial cells to limit cuprizone-induced demyelination

H.C. Hoyos [a,b], M. Rinaldi [a,b], S.P. Mendez-Huergo [c,d], M. Marder [a,b], G.A. Rabinovich [c,d,1], J.M. Pasquini [a,b,1], L.A. Pasquini [a,b,*,1]

[a] Department of Biological Chemistry, School of Pharmacy and Biochemistry, University of Buenos Aires and National Research Council (CONICET), Argentina
[b] Institute of Chemistry and Biological Physicochemistry (IQUIFIB), School of Pharmacy and Biochemistry, University of Buenos Aires and National Research Council (CONICET), Argentina
[c] Laboratory of Immunopathology, Institute of Biology and Experimental Medicine (IBYME; CONICET), C1428 Buenos Aires, Argentina
[d] Laboratory of Functional Glycomics, Departament of Biological Chemistry, School of Exact and Natural Sciences, University of Buenos Aires, C1428 Buenos Aires, Argentina

ARTICLE INFO

Article history:
Received 30 May 2013
Revised 10 October 2013
Accepted 23 October 2013
Available online 31 October 2013

Keywords:
Galectin-3
Demyelination
Cuprizone
Microglial phenotype
Oligodendroglial differentiation
TREM-2b

ABSTRACT

Galectin-3 (Gal-3) is a β-galactoside-binding lectin that plays an important role in inflammatory and neurodegenerative diseases. Cuprizone (CPZ)-induced demyelination is characterized by the loss of mature oligodendrocytes (OLG) by apoptosis, myelin sheath degeneration and recruitment of microglia and astrocytes to the lesioned area. We compared CPZ-induced demyelination of 8-week-old *Lgals3*$^{-/-}$ vs WT mice. *Lgals3*$^{-/-}$ mice displayed a similar susceptibility to CPZ-induced demyelination up to the fifth week, as evaluated by MBP immunostaining and electronic microscopy. However, OLG progenitors (OPC) generated in CPZ-treated *Lgals3*$^{-/-}$ mice showed diminished arborization, suggesting decreased ability of these cells to differentiate. Surprisingly, while WT mice experienced spontaneous remyelination in the fifth week of CPZ treatment—even though the CPZ diet was maintained up to sixth week—*Lgals3*$^{-/-}$ mice lacked this capacity and suffered continuous demyelination up to the sixth week, accompanied by pronounced astroglial activation. Moreover, after 2 weeks of CPZ treatment, WT and *Lgals3*$^{-/-}$ mice showed lower innate anxiety as compared with respective naive mice, but only CPZ-treated *Lgals3*$^{-/-}$ mice showed decreased locomotor activity and exhibited spatial working memory impairment. Expression of Gal-3 increased during CPZ-induced demyelination in microglia but not in astrocytes. While CPZ-treated WT mice displayed heightened microglial activation associated with ED1 expression and pronounced upregulation of the phagocytic receptor TREM-2b, this effect was not observed in CPZ-treated *Lgals3*$^{-/-}$ mice which, in spite of showing an increased number of microglia, these cells evidenced caspase-3 activation. Our results indicate that Gal-3 is expressed in microglial cells to modulate their phenotype, facilitating the onset of remyelination and OLG differentiation.

Introduction

Galectin-3 (Gal-3) belongs to an evolutionarily conserved family composed of 15 members which recognize β-galactosidase-containing glycans. This chimeric protein, structurally composed of unusual tandem repeats of proline and glycine-rich short stretches fused onto a carbohydrate-recognition domain (CRD), has multifaceted functions in many physiologic processes, including modulation of innate and adaptive immune responses (Rabinovich and Croci, 2012; Lalancette-Hébert et al., 2007; Nieminen et al., 2005; Rabinovich et al., 2007; Rotshenker, 2009; Sato and Nieminen, 2004; Sato et al., 2002). However, its role in central nervous system (CNS) immunity is poorly understood. Thus far, most in vitro and in vivo studies suggest that Gal-3 displays pro-inflammatory responses through its ability to promote immune cell activation, migration and inhibition of apoptosis (Rabinovich et al., 2007), although it has also been identified as a negative regulator of lipopolysaccharide-induced inflammation (Li et al., 2008). In the CNS, Gal-3 is up-regulated by inflammatory stimuli and plays a detrimental role in prion-infected brain tissue (Mok et al., 2006, 2007; Riemer et al., 2004). Recently, Lalancette-Hébert et al. (2012) demonstrated that Gal-3 plays a pivotal role in mediating injury-induced microglial activation and proliferation using a unilateral transient focal cerebral ischemia model in mice. In addition, when immunized with myelin oligodendrocyte (OLG) glycoprotein, *Lgals3*$^{-/-}$ mice showed lower severity of Experimental Autoimmune Encephalomyelitis (EAE) (Jiang et al., 2009), an animal model of CNS demyelination characterized by the expansion of encephalitogenic Th1 and Th17 cells (Langrish et al., 2005; Park et al., 2005; Weiner, 2008).

In contrast, the addition of cuprizone (CPZ) to the diet of young adult mice produces massive demyelination in different areas of the CNS, particularly in the corpus callosum (CC), through mechanisms that are independent of pathogenic T cells (Blakemore, 1973; Ludwin, 1978;

* Corresponding author at: Dpto de Qca Biol, FFyB-UBA, Junín 956, C1113, Buenos Aires, Argentina. Fax: +54 11 4962 5457.
E-mail address: laupasq@yahoo.com (L.A. Pasquini).
Available online on ScienceDirect (www.sciencedirect.com).
[1] These authors equally contributed to this work as co-senior authors.

0969-9961/$ – see front matter © 2013 Elsevier Inc. All rights reserved.
http://dx.doi.org/10.1016/j.nbd.2013.10.023

Matsushima and Morell, 2001; Suzuki and Kikkawa, 1969). In fact, CPZ-induced demyelination is characterized by the accumulation of resident microglia with few peripheral macrophages (McMahon et al., 2002). Greater myelin phagocytosis by microglial cells has been reported during CPZ-induced demyelination, which was associated with an up-regulation of phagocytic receptors among which TREM-2b was the most prominent (Voß et al., 2011). In this regard, phagocytosis of myelin debris by microglia and macrophages has been proposed to play an important role in the initiation of remyelination, as differentiation of oligodendrocyte precursor cells (OPC) can be inhibited by myelin (Kotter et al., 2006). Our previous studies have demonstrated that glial-derived Gal-3 promotes OLG differentiation and contributes to myelin integrity and function (Pasquini et al., 2011).

In the present study, we compared the susceptibility of adult *Lgals3*$^{-/-}$ and WT mice to CPZ-induced demyelination, their associated behavior and the dynamics of different cell types during the course of the demyelinating disease. Moreover, we analyzed the expression of maturation and phagocytic markers, cytokine production and microglial proliferation and death in both *Lgals3*$^{-/-}$ mice and their WT counterparts.

Experimental procedures

Animals and induced demyelination

Lgals3$^{-/-}$ mice (C57BL/6 background) were generously provided by Dr. F.-T. Liu (University of California, Davis) and generated as previously described (Hsu et al., 2000). Animals were housed in groups of 4 in a controlled environment (20–23 °C) with free access to food and water, and maintained on a 12 h-day/12 h-night cycle, with light on at 6 a.m. All animal protocols were approved by the Institutional Review Board of the University of Buenos Aires, and animal experimentation was in accordance with the National Institutes of Health Guide for the Care and Use of Laboratory Animals.

Experimental demyelination was induced by feeding 8-week-old male mice with 0.2% (w/w) cuprizone (CPZ, bis-cyclohexanone oxalhydrozone, Sigma) mixed into standard ground rodent chow (Matsushima and Morell, 2001). Animals were sacrificed 3, 4, 5 or 6 weeks after CPZ intoxication.

Tissue preparation

Animals were anesthetized with a xilazine–ketamine mixture and intracardially perfused with 30 ml PBS, pH 7.4, followed by 4% paraformaldehyde (PFA, Sigma Aldrich) in PBS, pH 7.4. Brains were carefully dissected out and post-fixed in the same solution overnight, and then thoroughly washed in PBS and cryoprotected in 30% sucrose in PBS. All brain slices (25 μm width) were kept at −20 °C in a PBS:glycerol solution (1:1) until they were selected for immunofluorescence studies.

Brain section selection

Previous to immunostaining assays, brain slices were selected using the Allen Mouse Brain Atlas (Lein et al., 2007) as a reference. The CC and subcallosal zone (SCZ) were studied in brain sections at the level of coronal slices 44–52 of the Atlas. After selection, brain slices were kept in PBS for immunohistochemical studies. For electron microscopy and flow cytometry assays (isolation of microglia), the CC was dissected out from brains kept in ice using a sterile razor blade. Dissection coordinates were +1.32 mm to +0.74 mm from Bregma, according to The Mouse Brain Library (online version), 2003. Immediately, the isolated CC were subjected to the procedure required for each particular method.

Immunohistochemistry

Cryotome sections were rinsed twice with PBS (pH 7.4) followed by an antigen blocking reagent composed of 5% FCS and 0.1% Triton X-100 in PBS. Primary and secondary antibody dilutions were prepared in 1% FCS and 0.1% Triton X-100 in PBS. Primary antibody incubation was done overnight at 4 °C. The primary antibodies used were rabbit anti-MBP (1/600), generously provided by Dr. A. Campagnoni (UCLA); anti-GFAP (1/100, Neuromics); anti-ED1 (1/100, Abcam); anti-Gal-3 (1/100), donated by Dr. F.-T. Liu (University of California, Davis); anti-CD11b (1/100, Abcam); anti-cleaved-caspase-3 (1/200, Neuromics); anti-PDGFRα (1/100, Neuromics); anti-Ly6C (1/100, Abcam); anti-Iba-1 (1/500, Abcam); and anti-CD45 (1/50, Neuromics). Incubation with Hoechst 33342 (Sigma Aldrich) and their respective fluorescent-conjugated antibodies (Alexa 488, Alexa 649, Cy2 and Cy3, Jackson Immunoresearch Lab) was done for 2 h at 37 °C with agitation. Lectin (GSA I-B4; 1/100, Vector Lab) was labeled with a Cy2-conjugated streptavidin. Slides were mounted and covered with Mowiol. Microphotographs were taken with an Olympus BX50 epifluorescent microscope connected to a CoolSnap digital camera. Image Pro Plus software (version 5.5) was used for image analysis. In all cases, measurements were carried out by experimenters who were blind to the experimental design. Images were identified with a number and, once measurements were done, image numbers were associated with each experimental condition. For the co-localization of a) Gal-3 with ED1 and GFAP and b) caspase-3 and CD11b, observations were carried out using an Olympus Fluorview FV1000 MPE multifoton microscope coupled to a Zeiss LSM 510 laser scanner. Merged versions and composite images were performed with FV10-ASW1.7 viewer software. Filament plot of PDGFRα and GFAP^{+} cells was obtained from z-stack scanning of cells at a slice distance of 0.75 μm using the IMARIS 6.3.1 program (Bitplane Sci Software) as described by Quinta and Galigniana (2012).

Cell proliferation assays

Mice from each experimental group were intraperitoneally injected with 5-bromo-2-deoxyuridine (BrdU; 100 mg/kg, Sigma) 24 h and 12 h before sacrifice. Cryotome sections were exposed for 30 min to a 2 N HCl solution with a rinse of 0.1 M borate buffer, pH 8.4, for 10 min. Immunohistochemical studies were performed following the procedure described above and using anti-BrdU (1/100, Roche), anti-Ki67 (1/100, Santa Cruz) and their respective secondary antibodies.

Western blot analyses

MBP isoforms, ED1 and GFAP were evaluated in CC cell extracts. Samples were resuspended and lysed in RIPA 1× (NaCl 300 mM, TRIS 20 mM, pH.7.4, SDS 0.2%) extraction buffer with a complete EDTA-free protease inhibitor cocktail (Roche). Equal amounts of protein were separated on SDS-PAGE and transferred onto PVDF membranes for Western blot analyses. Membranes were incubated with anti-MBP (1/1000), anti-ED1 (1/500) and anti-GFAP (1/1000) antibodies, followed by incubation with HRP-conjugated antibodies. Quantification was done by densitometry with the Gel Pro Analyzer 4.0 system.

Electron microscopy (EM)

Four to six animals per group were decapitated at 5 weeks of treatment. CC was dissected out as described above, fixed and immediately prepared for EM. Ultrathin cuts were examined using a Zeiss Leo 906 E electron microscope equipped with a Zeiss Megaview III digital camera. Parameters assessed included: a) percentage of correctly myelinated axons per field; b) g-ratio (the ratio between the axon's diameter and the axon's diameter wrapped with myelin) and c) number of myelin turns around an axon. Images were analyzed by experimenters who were blind to the experimental design. Eight images were obtained for

each experimental condition. The number of myelinated axons per field was determined by counting the axons in each image (magnification 6000×), and then classifying them according to their demyelination state and axon diameter. The g-ratio was evaluated in 12 axons per image, by means of the Image-J software. Myelin turns were quantified in high magnification images (magnification 85,000×).

Isolation of microglia

Anaesthetized animals were transcardially perfused with ice-cold PBS to clear the intravascular compartments from blood cells. CC were dissected out as previously described and transferred to Hank's solution buffer (HBSS) without Ca^{+2} and Mg^{+2}. CC plus cortex (CX) were chopped in small pieces and centrifuged at 4 °C at 300 ×g for 2 min. Cells were then selected using a separation column kit (Cat# 130-093-634, MACS Miltenyi Biotec) with anti-CD11b labeled with magnetic microbeads. The separation protocol was carried out according to the manufacturer's instructions. After removing the column from the magnetic field, retained $CD11b^{+}$ cells were eluted as the positively-selected cell fraction. This fraction was separated into 7 different tubes with an equal number of cells. Six of these tubes were incubated for 30 min at 37 °C with antibodies labeled with specific fluorosphores: anti CD11b-PE, CD45-FITC, TNF-PE, CD200-PE, MHC II-FITC (all from eBioscience) and anti-TREM/2-PE (R&D System), following the suppliers' instructions. The seventh sample was fixed for 30 min with 4% PFA, rinsed once with PBS and treated with 2 N HCl for 30 min and a rinse with 0.1 M borate buffer, pH 8.4. After this treatment, samples were incubated with an anti-BrdU antibody (Roche) and its respective secondary antibody. Finally, all samples were analyzed with a flow cytometer (Beckmann) and results were expressed using WinMDI 2.8 software.

Behavioral tests

At the second and fifth weeks of CPZ-induced demyelination, 12 mice per group were subjected to behavioral studies. Tests were performed between 10:00 a.m and 2:00 p.m in an arrangement of 24 h in between behavioral tests. The following studies were performed: plus-maze, locomotor activity, hole-board, inverted screen and Y-maze tests to measure anxiety, locomotor activity, exploration, motor coordination and spatial working memory, respectively. In all cases, investigators were blind to experimental conditions. After each experiment, all devices were wiped clean to remove traces of the previous assay.

Elevated plus-maze test

The elevated plus-maze set-up consisted of a maze of two open arms, 25 × 5 cm, crossed by two closed arms of the same dimensions, with free access to all arms from the crossing point. The closed arms had walls 15 cm high all around. The maze was suspended 50 cm from the room floor. Mice were placed on the central part of the cross facing an open arm. The number of entries and the time spent going into open arms were counted during 5 min under red dim light. The total exploratory activity (number of entries in both arms) was also determined (Lister, 1987).

Hole-board assay

This assay was conducted in a black walled Plexiglas arena with a floor of 60 × 60 cm and 30 cm high walls, with four centered and equally spaced holes on the floor, with a diameter of 2 cm each, as previously described (Fernández et al., 2006), and illuminated by a dim indirect light. Each animal was placed in the center of the holeboard and allowed to freely explore the apparatus for 5 min; the number of holes explored, the time spent head dipping and the number of rearings was then measured.

Locomotor activity test

The spontaneous locomotion activity was measured in a box made of Plexiglas, with a floor of 30 × 15 cm and 15-cm-high walls, as previously described (Fernández et al., 2006). The locomotor activity was expressed as total light beam counts per 5 min.

Inverted screen test

The inverted screen test was used to assess motor coordination (Coughenour et al., 1977). Mice were placed on a 13 × 13-cm wire mesh screen elevated 40 cm above the ground. After slowly inverting the screen through an angle of 180°, the time required for each mouse to climb to the top was recorded, as was the number of mice that dropped off. Mice not climbing to the top (all four paws on upper surface) were counted as failures. A 150-second cut-off was imposed. The inverted screen test is a functional test that requires coordination and strength. Occasionally, mice need to be trained to climb over the edge of the screen, but mice used here were not pre-tested.

Y maze test

The experimental apparatus consisted of a Y-maze made of gray Plexiglas with three identical arms mounted at 120° to one another. Each arm of the Y-maze was 32.5-cm long, 15-cm high and 8.5-cm wide (labeled A, B and C). Each mouse was placed at the end of one arm and allowed to move freely through the maze during an 8-min test period. The sequence of arm entries was recorded manually (that is, ABCBAC, and so on). An actual alternation was defined as entries into all three arms on consecutive occasions. Therefore, the maximum alternation was defined as the total number of arm entries minus two, and the percentage of alternation was calculated as (actual alternations / maximum alternations) / 100. The total number of arms entered during the sessions was also determined. Continuous spontaneous alternation behavior in the Y-maze was a measure to assess short term spatial memory (Dellu et al., 2000).

Real-time quantitative RT-PCR

SYBR Green PCR Master Mix was used with an ABI PRISM 7500 Sequence Detection Software (all from Applied Biosystems). Primers used were: mouse GAPDH, forward: CCAGAACATCATCCCTGCAT, reverse: GTTCAGCTCTGGGATGACCTT; mouse Ccl-2 (MCP-1), forward: CACTCACCTGCTGCTACTCA, reverse: GCTTGGTGACAAAAACTACAGC; mouse M-CSF, forward: AAGGCCTGTGTCCGAACTTT, reverse: TGGTC ACCACATCTCGGCTA.

Statistical analyses

Graph-Pad Prism Software was used for data analysis. Results were presented as mean ± SEM. Comparisons were performed using unpaired one-tailed Student's *t*-test or one way analysis of variance (ANOVA) followed by Bonferroni post-hoc tests where appropriate. Data from behavioral assays were analyzed by two-way ANOVA, considering CPZ treatment and animal type as two main factors, and post-hoc comparison was made using Bonferroni post test. When a significant interaction was observed, subsequent one-way ANOVA and Newman–Keuls Multiple Comparison post-hoc test was applied. $P < 0.05$ was considered statistically significant.

Results

Susceptibility of $Lgals3^{-/-}$ mice to CPZ-induced demyelination and ability to initiate spontaneous remyelination

$Lgals3^{-/-}$ mice (C57BL/6 background) were generously provided by Dr. F.-T. Liu (University of California, Davis) and generated as described (Hsu et al., 2000). Animals were housed in groups of 4 in a controlled environment (20–23 °C) with free access to food and water, and

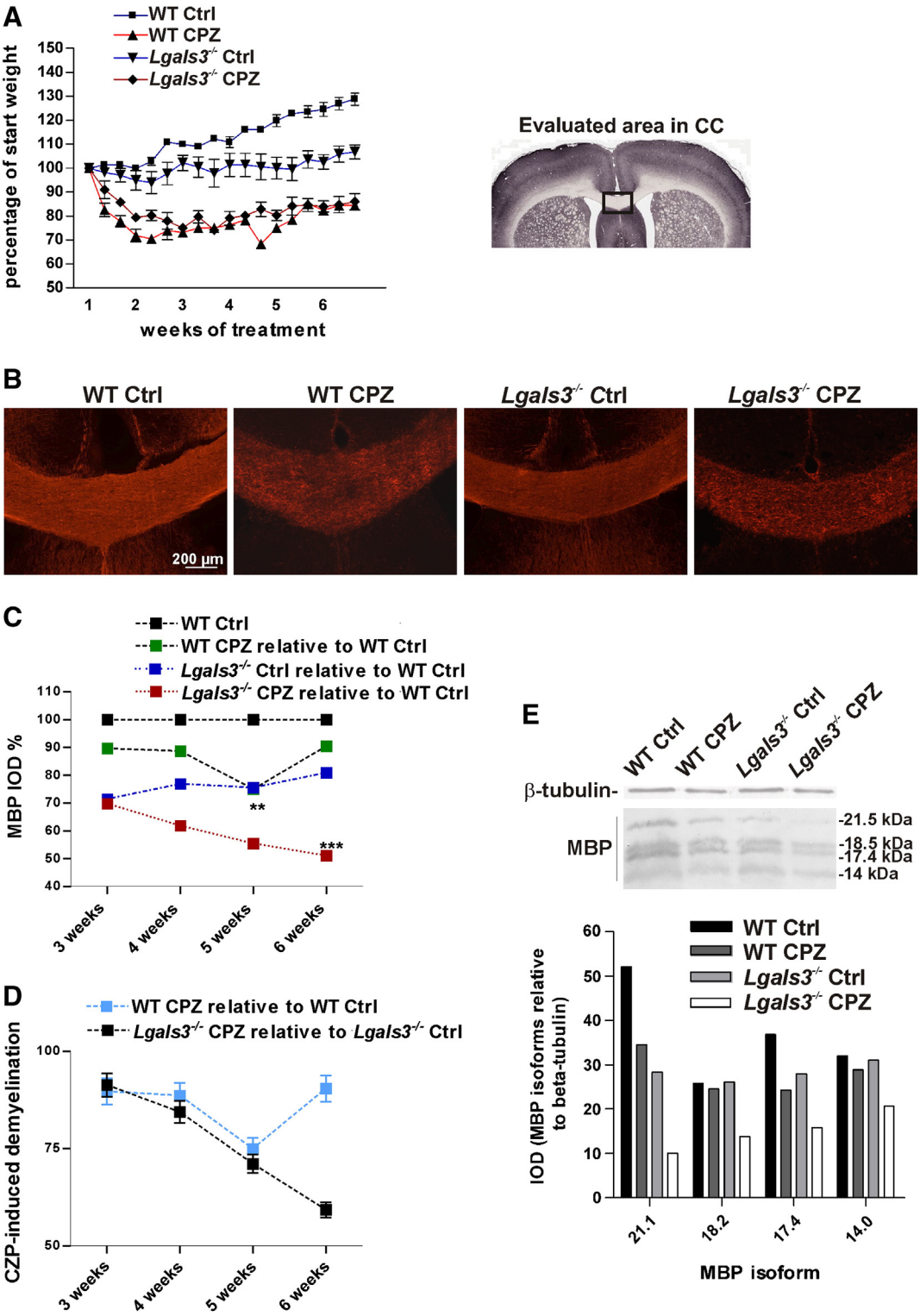

Fig. 1. CPZ-induced demyelination. A: Weight variation during treatment. Animal weight before treatment was regarded as 100%. At least 15 animals per group were measured in each time point. B: Representative sections showing MBP expression in stained CC sections at the fifth week of treatment. C: Immunoreactive signal was measured by IOD in a grid of several rectangles within the medial CC, as detailed in the scheme (box), using the Image Pro Plus 5.5 Software. Images (magnification 20×) were measured from 4 to 5 mice per treatment per time point. Demyelination score measured by MBP IOD relative to WT Ctrol was assumed as 100%. WT CPZ mice experienced demyelination until the 5th week of treatment, when they started to spontaneously remyelinate. Ctrol l-fed-*Lgals3*$^{-/-}$ mice exhibited hypomyelination and CPZ-fed-*Lgals3*$^{-/-}$ mice suffered sustained demyelination without spontaneous remyelination. D: Demyelination rate during treatment of WT CPZ relative to WT Ctrol and *Lgals3*$^{-/-}$ CPZ relative to *Lgals3*$^{-/-}$ Ctrol. These rates revealed equal susceptibility to CPZ demyelination in both animal strains, although only WT mice were able to spontaneously remyelinate. E: Western blot analysis of MBP expression provided quantitative support for panels B and C. Note that not all MBP isoforms are equally affected, 21.1 and 17.4 kDa isoforms being the most affected ones. β-tubulin was used as a loading control. Values represent the mean ± SEM of 3 independent experiments. **P < 0.01; ***P < 0.001 using one way analysis of variance (ANOVA) followed by Bonferroni post-hoc tests.

maintained on a 12 h/12 h day/night cycle, with lights on at 6 a.m. All animal protocols were approved by the Institutional Review Board of the University of Buenos Aires, and animal experimentation was in accordance with the National Institutes of Health Guide for the Care and Use of Laboratory Animals.

In order to evaluate the course and extent of demyelination induced by CPZ treatment during 3, 4, 5 or 6 weeks, brain coronal sections of *Lgals3*$^{-/-}$ and WT mice were histochemically stained for the myelin basic protein (MBP) (Fig. 1B). In WT animals, MBP immunoreactivity decreased continuously under CPZ treatment, reaching a minimum around the fifth week. At that time, spontaneous remyelination was initiated even though the CPZ diet was maintained up to the sixth week. In agreement with our previously published data (Pasquini et al., 2011), *Lgals3*$^{-/-}$ mice showed basal hypomyelination relative to WT mice. In contrast to WT mice, *Lgals3*$^{-/-}$ mice subjected to the CPZ diet developed continuous demyelination during the observation period (up to the sixth week), with no signs of remyelination. Quantitative support was obtained through Integrated Optical Density (IOD) of MBP immunoreactivity in the CC of the different experimental conditions relative to control-fed WT mice (Fig. 1C). To evaluate whether mice lacking Gal-3 were differentially susceptible to CPZ-induced demyelination, data were expressed as an IOD ratio in CPZ-treated vs control-fed WT mice or in CPZ-treated vs control-fed *Lgals3*$^{-/-}$ mice (Fig. 1D). Our results showed a similar decrease in MBP myelinated tracts in the CC following CPZ treatment in WT and *Lgals3*$^{-/-}$ mice up to the fifth week, when the remyelination process started only in WT mice (Fig. 1D). These data reflect a similar susceptibility to CPZ-induced demyelination in both animal strains but a differential capacity to initiate the remyelination process. Western blot analyses of MBP expression in the CC provided semiquantitative support to immunohistochemical studies (Fig. 1E).

The number of OPC labeled for PDGFRα was higher in both CC and SCZ from *Lgals3*$^{-/-}$ compared to WT mice previous to CPZ treatment, suggesting an oligodendroglial proliferative response to basal hypomyelination. When both animal strains were submitted to CPZ intoxication, a significant increase was observed in the number of PDGFRα^{+} cells (Fig. 2A), which was higher in *Lgals3*$^{-/-}$ mice as a consequence of stronger demyelination. Interestingly, these cells showed a stellate morphology with a higher number of multipolar processes in WT mice (Fig. 2B), indicating a decreased ability of *Lgals3*$^{-/-}$ cells to differentiate. Quantitative support was obtained through the assessment of branches and terminal processes as well as their length (Fig. 2B).

To assess changes in myelination at the ultrastructural level, we used transmission transmission electron microscopy in CC from *Lgals3*$^{-/-}$ and WT mice subjected to 5 weeks of CPZ treatment. *Lgals3*$^{-/-}$ mice

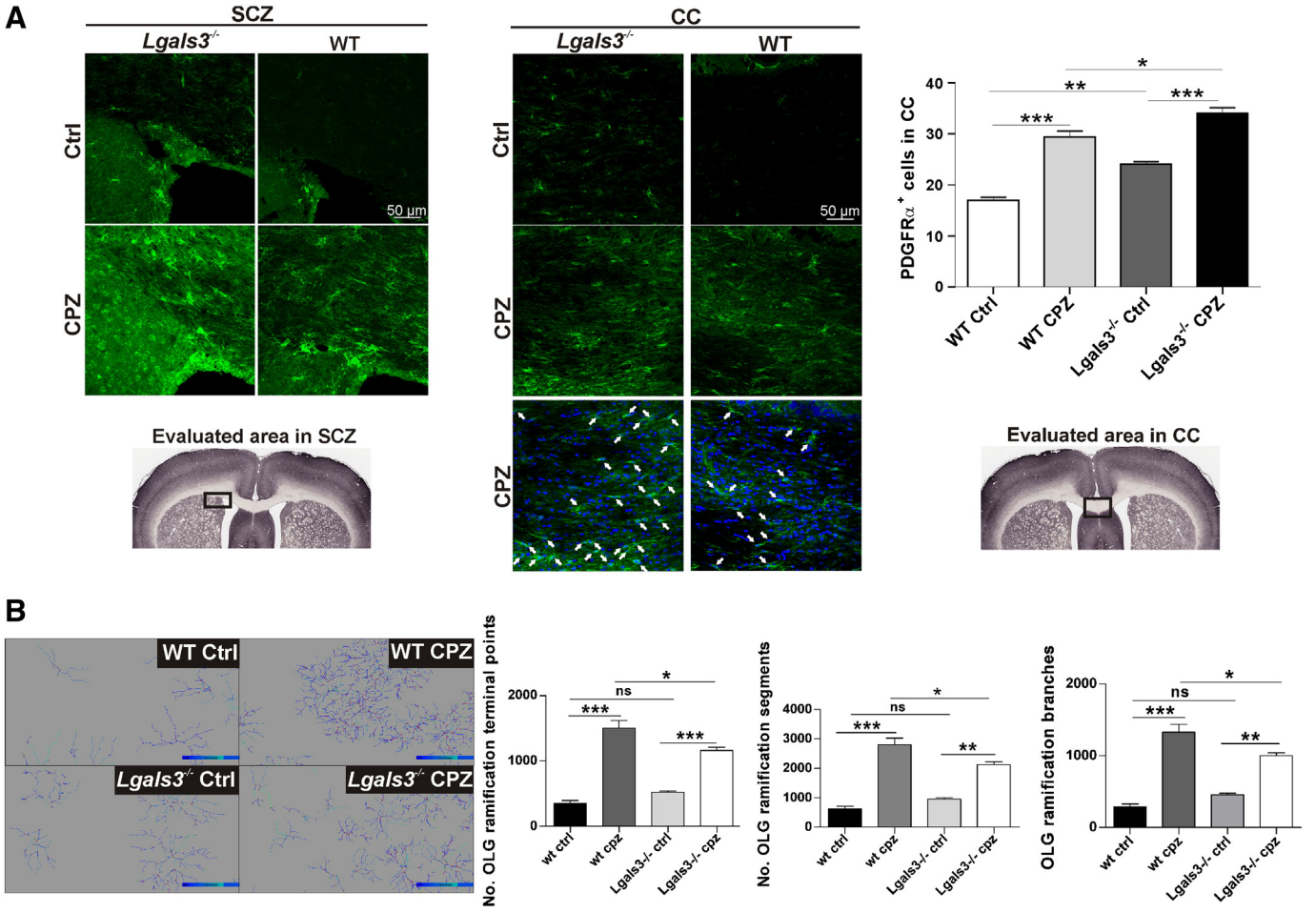

Fig. 2. Identification of OPC after CPZ treatment. A: OPC were identified as PDGFRα^{+} cells in SCZ and CC (white arrows). Images obtained by confocal microscopy in the z axis were reconstructed to obtain a 3D figure using Image J software (z-stack). PDGFRα^{+} cells were quantified in the CC within the scheme boxes depicted in the figure. Measurements were done using the IMARIS 6.3.1 program (Bitplane Sci Software), which determines the cell soma and its projections. The number of cell soma was taken as the number of PDGFRα^{+} cells. Images (magnification 20× and 40×) were measured from 4 to 5 mice per treatment per time point. Quantification shown in the right graph revealed an increase in the number of PDGFRα^{+} cells in CC in both animals fed with CPZ, although this increase was greater in *Lgals3*$^{-/-}$ mice. B: Filament plot was performed for each image and quantification is shown on the right bar graph. Values represent the mean ± SEM of 3 independent experiments. PDGFRα^{+} cells exhibit greater arborization in WT CPZ than in *Lgals3*$^{-/-}$ CPZ mice. ns: non-significant; *P < 0.05; **P < 0.01; ***P < 0.001 using oneway analysis of variance (ANOVA) followed by Bonferroni post-hoc tests.

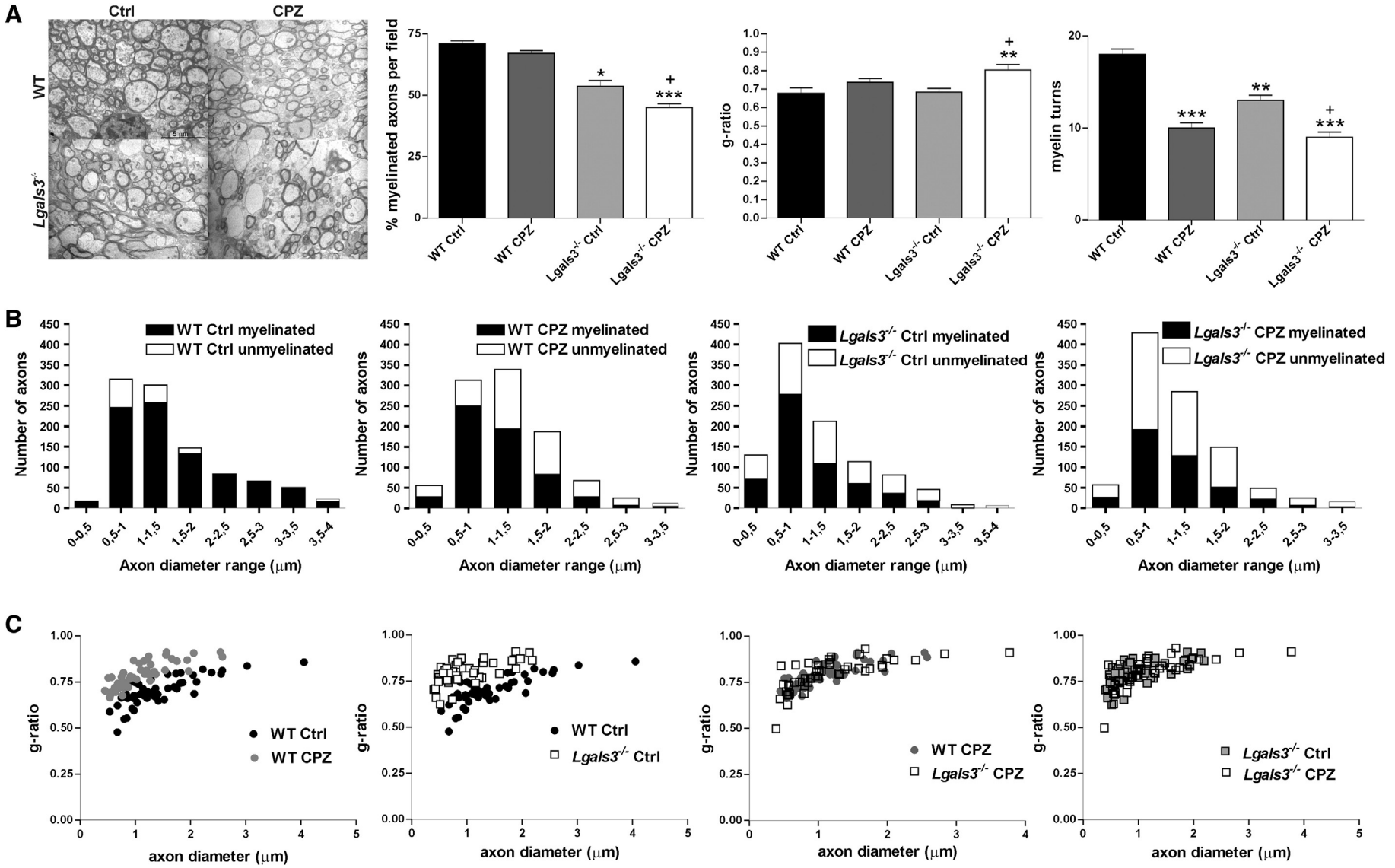

Fig. 3. EM studies of myelin structure in WT and *Lgals3*$^{-/-}$ mice. A: Representative EM photographs at 6000×, with a scale bar equal to 5 μm. Myelin obtained from *Lgals3*$^{-/-}$ mice is loosely wrapped around the axons as compared to myelin from WT mice. Morphometric analysis shows the percentage of correctly myelinated axons, the number of myelin turns and the g-ratio. The symbols denote significance: *, relative to WT Ctrol and +, relative to *Lgals3*$^{-/-}$ Ctrol. B: Relationship between axon caliber and state of myelination. C: G-ratio distribution plotted versus axon diameter. At least 3 mice per experimental condition and 12 images for each mouse were analyzed. Values are expressed as the mean ± SEM. Comparisons were performed using unpaired one-tailed Student's *t*-test (+ and *P < 0.05; **P < 0.01; ***P < 0.001).

showed a significant decrease in the percentage of myelinated axons and myelin turns relative to WT mice (Fig. 3A). Morphometric analyses showed that CPZ treatment induced a significant decrease in the number of myelinated axons per field and myelin turns (lamellae) in *Lgals3*$^{-/-}$ mice, together with an increase in the g-ratio (Fig. 3A). When these parameters were expressed as ratios between CPZ- and control-fed animals, results showed similar vulnerability to CPZ treatment in both animal strains (data not shown). These results are in agreement with immunohistochemical studies for MBP expression, except for the evaluation of myelin turns, where WT seemed to be more widely affected. Thus, basal hypomyelination in *Lgals3*$^{-/-}$ mice might allow only for a slight loss of lamellae which is compatible with life. When the relationship between axonal caliber and state of myelination was evaluated, results showed a higher number of smaller axons and demyelinated axons distributed in all ranges of diameter sizes in control-fed *Lgals3*$^{-/-}$ mice as compared to their WT counterpart (Fig. 3B). In WT mice, CPZ treatment induced a significant increase in the number of small axons, concomitantly with a decrease in large ones. In contrast, in *Lgals3*$^{-/-}$ mice CPZ treatment led to a loss of small axons, an effect probably associated with the basal demyelinated status of these mice, which led to degeneration under induced demyelination. Accordingly, when g-ratios were plotted versus axonal diameters, control-fed *Lgals3*$^{-/-}$ mice showed a larger number of axons with small diameter and g-ratio closer to 1 relative to WT mice, which reflects basal hypomyelination in Gal-3-deficient mice. Moreover, CPZ-treated WT mice evidenced a shift of g-ratio/axon diameter parameters toward smaller axons and g-ratios closer to 1, while *Lgals3*$^{-/-}$ mice displayed a substantial overlap of both parameters (Fig. 3C). Thus, CPZ treatment favored the loss of large axons and promoted an increase in the number of small demyelinated axons in WT mice, while *Lgals3*$^{-/-}$ mice were extensively affected in accordance with their basal hypomyelination status.

Lgals3$^{-/-}$ *mice display heightened astroglial response*

Reactive astrogliosis was observed by glial acidic fibrillary protein (GFAP) staining in response to CPZ treatment. The astroglial response was more sharply augmented in *Lgals3*$^{-/-}$ mice with demyelination still under way at the sixth week of CPZ treatment, when the remyelination process started in WT animals (Fig. 4A). These data were supported by semiquantification of GFAP + cells in the CC and Western blot analyses (Figs. 4B and C). GFAP staining, evaluated in the sixth week of CPZ treatment, showed considerable changes in astroglial morphology. In fact, astrocytes of *Lgals3*$^{-/-}$ mice displayed hypertrophic processes with a sharp increase in ramification terminal points, segments and branches (Fig. 4D).

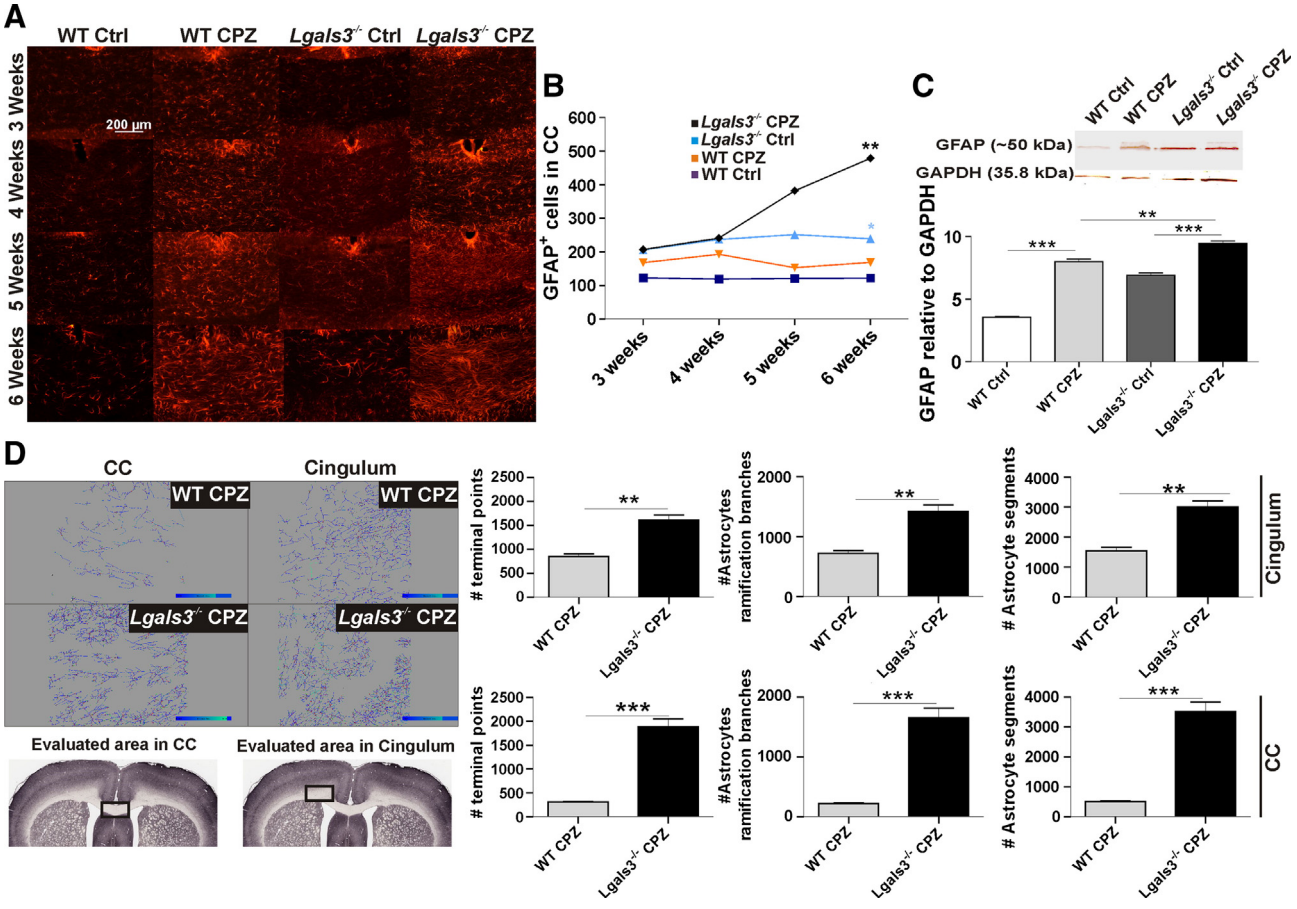

Fig. 4. The astroglial compartment in response to CPZ-induced demyelination under Gal-3 deficiency. A: Astrocytes immunostained with anti-GFAP antibody in the CC in response to CPZ treatment in WT or *Lgals3*$^{-/-}$ animals. The astroglial response was particularly increased in *Lgals3*$^{-/-}$ mice in the sixth week of CPZ treatment, when the remyelination process started in WT animals. B: GFAP^{+} cells were quantified in the CC within the scheme boxes depicted in the figure. Measurements were done using the IMARIS 6.3.1 program (Bitplane Sci Software), which determines the cell soma and its projections. The number of cell soma was taken as the number of GFAP^{+} cells. Images (magnification 20× and 40×) were measured from 4 to 5 mice per treatment per time point. Quantification of GFAP^{+} cells evaluated in relationship with WT Ctrl condition, assumed as 100%. C: Western blot analysis of GFAP expression at the fifth week of intoxication. The graph below shows GFAP quantification relative to GAPDH. D: Filament plot was performed in the sixth week of CPZ treatment for each image and quantification is shown on the right bar graph. Values represent the mean ± SEM of 4 independent experiments. GFAP^{+} cells exhibit greater arborization in *Lgals3*$^{-/-}$ CPZ than WT CPZ mice in both CC and Cingulum. ns: non significant; *P < 0.05; **P < 0.01; ***P < 0.001 using unpaired one-tailed Student's *t*-test followed by Bonferroni post-hoc tests.

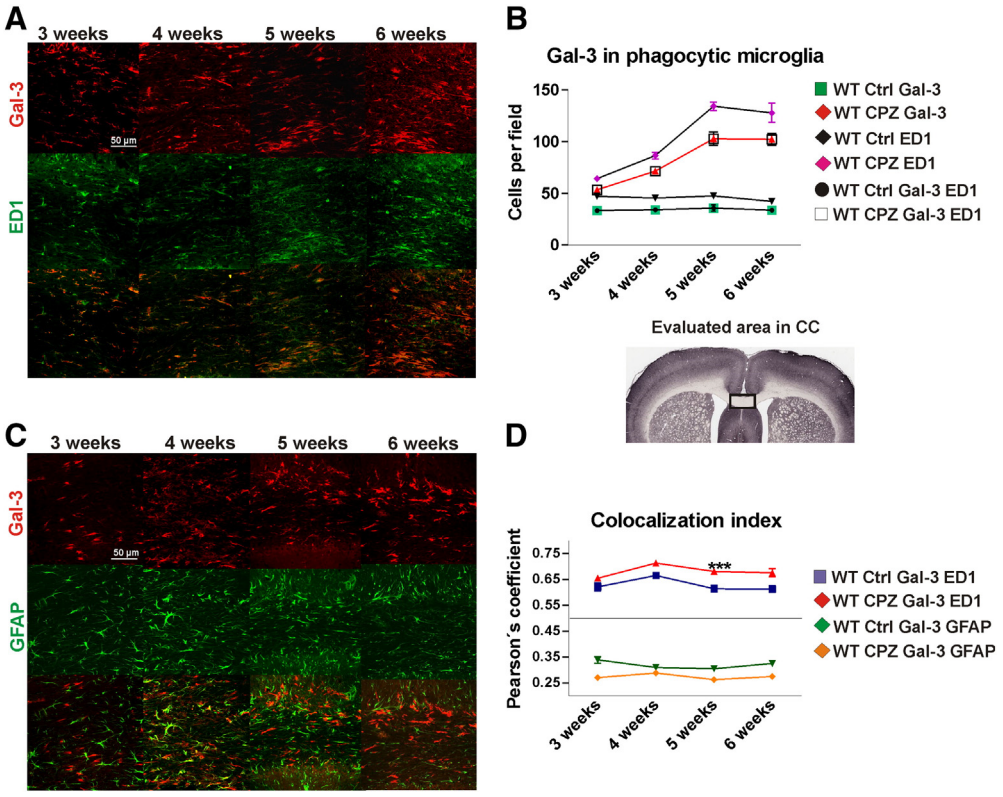

Fig. 5. Co-localization of Gal-3 with ED1 (activated microglia) or GFAP (astrocytes) during CPZ-induced demyelination. A and C: Confocal micrographs of CC of WT mice during CPZ treatment. In panel A, some ED1$^+$ cells (green) co-localized with Gal-3$^+$ cells (red) and merged cells were distinguished as orange ones (white arrows). In panel C, GFAP$^+$ cells (green) had no co-localization with Gal-3$^+$ cells (red). B: Quantification of ED1$^+$, Gal-3$^+$ and ED1$^+$/Gal-3$^+$ cells during CPZ treatment in WT mice. Cell quantification was determined in the scheme boxes within the CC. A peak in ED1$^+$/Gal-3$^+$ cells was observed in the fifth week of treatment. D: Co-localization was assessed using an application from Image Pro Plus 5.5 Software which calculates the co-localization index. The scheme shows the co-localization index using Pearson's coefficient (referring to the measure over 0.5). ED1 and Gal-3 showed significant co-localization but GFAP and Gal-3 did not. Statistical comparisons were performed using unpaired one-tailed Student's *t*-test, n ≥ 4 (ns: non-significant; *P < 0.05; **P < 0.01; ***P < 0.001).

Gal-3 is expressed in activated microglial cells during CPZ-induced demyelination

CPZ administration induces rapid proliferation and accumulation of microglia and macrophages in the CC (Hiremath et al., 1998; Morell et al., 1998), which is necessary for demyelination (Pasquini et al., 2007). To evaluate the temporal course of Gal-3 expression and its cellular localization, co-immunostaining was carried out using an anti-Gal-3 antibody and specific markers of activated microglia (ED1) or astrocytes (GFAP) during CPZ-induced demyelination. Confocal micrographs showed that all Gal-3$^+$ cells were positive for ED1 from the third week, showing a peak in the fifth week of intoxication, while the presence of ED1$^+$/Gal-3$^-$ cells was also detected (Figs. 5A, B and D). In contrast, no co-localization of GFAP and Gal-3 expression was observed (Figs. 5C and D). In agreement with these results, recent studies showed that Gal-3 expression was detectable at five weeks of CPZ diet on microglial cells in the CC and remained elevated during remyelination (Olah et al., 2012).

Gal-3 is required for microglial activation

To evaluate the involvement of microglial cells in Gal-3-mediated effects, we first stained the CC of animals subjected to different experimental conditions using the specific lectin *Griffonia simplicifolia*. In agreement with previous studies, WT mice fed with a control diet evidenced a small number of microglial cells with an increase in *Griffonia* IOD as from the third week of CPZ intoxication (Supplementary Fig. 1). Remarkably, control-fed and CPZ-fed *Lgals3*$^{-/-}$ mice showed higher levels of *Griffonia* IOD and a substantial increase in microglial activation relative to control-fed WT mice (Supplementary Fig. 1).

To examine the effects of Gal-3 on microglial activation during CPZ-induced demyelination, total and activated/phagocytic microglia were determined as CD11b$^+$ cells and ED1$^+$ cells, respectively. The number and intensity of CD11b$^+$ cells increased substantially from the third week of CPZ treatment in both WT and *Lgals3*$^{-/-}$ mice, although this increase was greater in *Lgals3*$^{-/-}$ than in WT mice (Figs. 6A and B). To determine the viability of CD11b$^+$ cells, studies of co-localization of CD11b and cleaved caspase-3 were performed in the fifth week of CPZ treatment. A significant increase in the number of double positive CD11b$^+$/cleaved caspase-3$^+$ cells was observed in *Lgals3*$^{-/-}$ relative to WT mice (Figs. 6A and C). Analyses of the phagocytic capacity of microglial cells revealed that CPZ treatment induced a robust upregulation of ED1 only in WT mice, while ED1$^+$ cells were absent in *Lgals3*$^{-/-}$ mice (Fig. 6D). Quantitative support was obtained from immunoprecipitation of CC total lysates using an ED1 antibody and Western blot analyses, which enabled concentration of samples and detection of ED1 reactivity. Quantitative results showed an increase in ED1 immunoreactivity only in WT mice treated with CPZ during 5 weeks (Fig. 6E). Our results suggest that Gal-3 is required for demyelination-induced microglial activation. To expand our analysis to other areas of the brain, Iba-1 immunoreactivity was evaluated in the whole coronal slices, and in a specific structure distinct from the CC, namely the CX (Fig. 7A). To this end, a quantitative assessment of the number and length of branches and terminal processes was conducted. In agreement with CD11b immunoreactivity, results showed an increase in Iba-1 immunoreactivity in CPZ-treated *Lgals3*$^{-/-}$ mice relative to CPZ-treated WT mice. When the CX was specifically evaluated, no changes were observed in the segments, terminal points or branches of the Iba-1$^+$ cells analyzed, which suggests that the absence of Gal-3 does not affect microglial activation in areas presenting lower quantities of myelin debris to phagocyte (Fig. 7B).

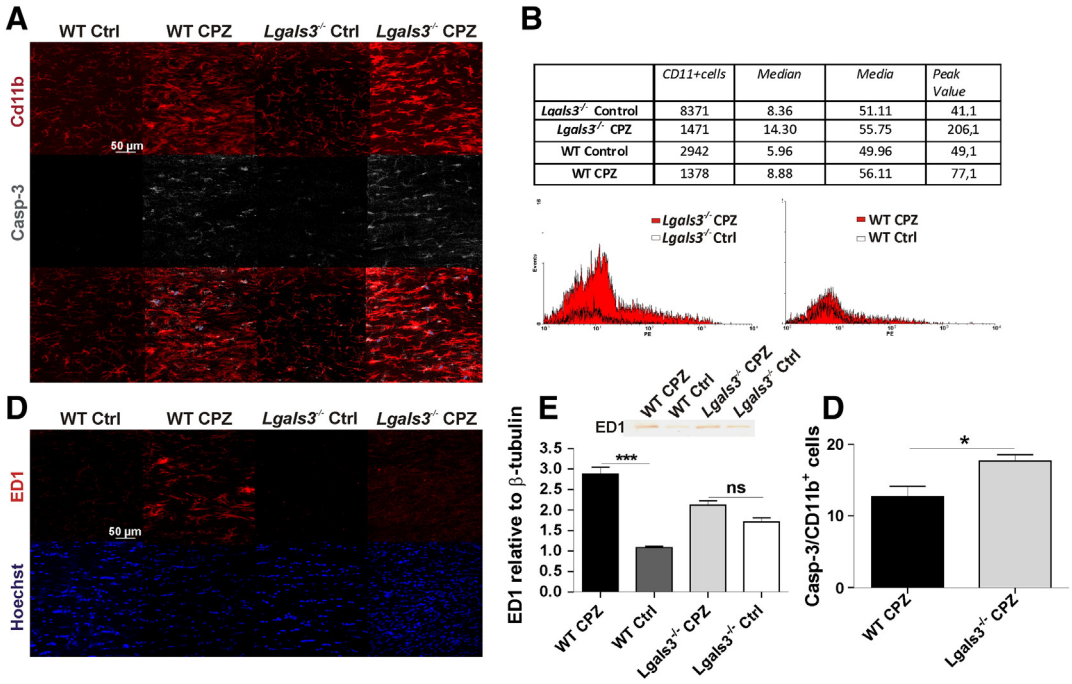

Fig. 6. Evaluation of microglial activation in the fifth week of CPZ-induced demyelination in WT and *Lgals3*$^{-/-}$ mice. A: Images of CC obtained by confocal microscopy in the fifth week of treatment. Total microglia was determined as CD11b^{+} cells. Apoptotic cells were evidenced by cleaved Casp3 (caspase-3). Co-localization of CD11b and cleaved Casp3 was assessed to determine microglial apoptosis. B: Representative flow cytometry histograms and quantitative assessment of the frequency of CD11b^{+} cells; on the left, *Lgals3*$^{-/-}$ CPZ (red) vs. *Lgals3*$^{-/-}$ Ctrl (white) and, on the right, WT CPZ (red) vs. WT Ctrl (white). CD11b^{+} cells were isolated with magnetic microbeads conjugated with an antibody against CD11b, immunostained with a PE-conjugated anti-CD11b-PE antibody and analyzed by flow cytometry (Beckmann). Data were processed with Winmdi 2.8 Software. C: Quantification of co-localization of CD11b^{+}/cleaved Casp3^{+} cells from WT CPZ and *Lgals3*$^{-/-}$ CPZ mice. D: Activated/phagocytic microglia were determined as ED1^{+} cells in the fifth week of treatment. E: Western blot analysis of immunoreactive ED1 protein bands. Quantitative support was obtained from immunoprecipitation of CC total lysates using an anti-ED1 antibody. The graph below shows ED1 quantification relative to β-tubulin (loading control). Values represent the mean ± SEM of 3 independent experiments. *P < 0.05, **P < 0.01; ***P < 0.001 using one way analysis of variance (ANOVA) followed by Bonferroni post-hoc tests.

Cell proliferation was evaluated by immunofluorescence for Ki67, a marker of proliferating cells and incorporation of BrdU in the CC of WT and *Lgals3*$^{-/-}$ mice during CPZ-induced demyelination (Fig. 8A). Quantitative studies of BrdU^{+} cells during demyelination in the CC revealed a marked increase in the number of proliferating cells in both animals, as compared to the weak proliferation present in control WT and *Lgals3*$^{-/-}$ mice. However, *Lgals3*$^{-/-}$ mice reached a maximum of proliferation earlier than WT mice (Fig. 8B). When incorporation of BrdU was assessed in CD11b^{+} cells, previously selected by separation with magnetic microbeads, quantification showed a higher number of CD11b^{+}/BrdU^{+} cells in control-fed *Lgals3*$^{-/-}$ relative to WT mice. Moreover, the number of CD11b^{+}/BrdU^{+} cells was higher in CPZ-fed *Lgals3*$^{-/-}$ than in WT mice in both the fourth and fifth weeks of intoxication. Moreover, CPZ-fed *Lgals3*$^{-/-}$ mice displayed a decrease in the number of these cells from the fourth to the fifth week while CPZ-fed WT mice exhibited no considerable changes (Fig. 8C).

Gal-3 imprints a microglial phagocytic phenotype during CPZ-induced demyelination

A pronounced increase in the phagocytic capacity of microglial cells has been reported during CPZ-induced demyelination, associated mainly with an upregulation of the phagocytic receptor TREM-2b (Voß et al., 2011). To study whether Gal-3 expression participates in the induction of this phagocytic receptor, we used magnetic microbeads to isolate CD11b^{+} cells from *Lgals3*$^{-/-}$ and WT mice in the fourth and fifth weeks of CPZ treatment. These animals were previously perfused with ice-cold PBS to clear the intravascular compartment from blood cells. In agreement with previously published data, CPZ-fed WT mice displayed upregulation of TREM-2b as from the fifth week of CPZ-treatment. Surprisingly, *Lgals3*$^{-/-}$ mice were unable to induce TREM-2b (Fig. 9A). Original representative FACS plots are shown in Supplementary Fig. 2, in which the cut-off was determined according to pre-incubation with pre-immune sera.

To further characterize the microglial phenotype, we studied the expression of MHC class II, CD200R—a receptor that mediates inhibitory signals in microglial cells—and TNF-α—a pro-inflammatory cytokine. Our results showed unaltered MHC II expression in both *Lgals3*$^{-/-}$ and WT mice subjected to 4 or 5 weeks of CPZ intoxication. On the other hand, WT mice exhibited non-significant upregulation of CD200R expression early during CPZ-induced demyelination (fourth week), followed by a substantial downregulation of this receptor in the fifth week. In contrast, *Lgals3*$^{-/-}$ mice were unable to upregulate CD200R in the fourth or fifth weeks, and displayed a significant down-regulation starting from the fourth week. Finally, we found increased production of TNF-α in microglial cells from WT mice, although these changes were not statistically significant. In turn, *Lgals3*$^{-/-}$ mice showed unaltered TNF-α production during the fourth and fifth weeks of CPZ treatment. Interestingly, TNF-α production in the fifth week of CPZ treatment was significantly higher in WT than in *Lgals3*$^{-/-}$ mice (Fig. 9A).

Isolated CD11b^{+} cells were stained for CD45 and CD11b expression in order to differentiate between microglia and macrophages. Microglia typically express a CD11b^{+}/CD45^{low} phenotype, while macrophages are typically CD11b^{+}/CD45^{high} (Ford et al., 1995; Sedgwick et al., 1991). A higher number of CD11b^{+}/CD45^{high} cells were found in the fourth week of CPZ treatment in both *Lgals3*$^{-/-}$ and WT mice, although this increase was only statistically significant in *Lgals3*$^{-/-}$ mice (Fig. 9A). When CD11b^{+}/CD45^{high*} cells were selected using a cut-off demanding higher levels of CD45 expression, the number of these cells showed a more pronounced increase in CPZ-treated *Lgals3*$^{-/-}$ vs WT mice, 3.4 ± 1.0 vs. 1.1 ± 0.9 (Fig. 7B). CD11b^{+}/CD45^{high} were also positive

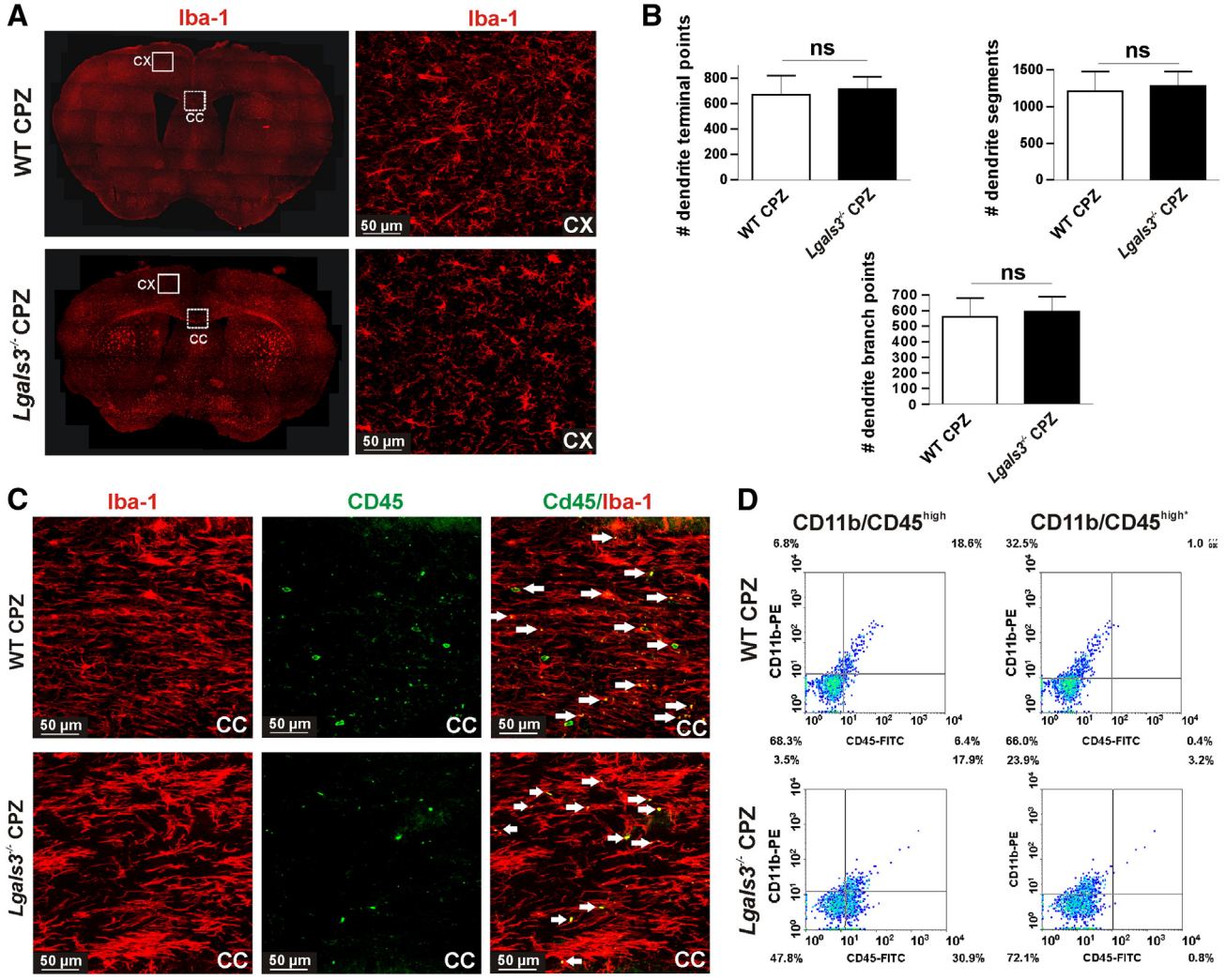

Fig. 7. A: Immunostaining of Iba-1 in coronal brain slices in the fifth week of CPZ-induced demyelination in WT and *Lgals3*$^{-/-}$ mice. Carefully matched adjoining photographs obtained from a single brain section were used to prepare an Iba-1 composite photograph. Iba-1 immunohistochemistry in CX. Microscopic studies were done in the area delineated by a continuous box (CX). Images from CX were obtained by confocal microscopy in the z axis and were reconstructed to obtain a 3D figure using Image J software (z-stack). B: Filament plot was performed for each z-stack of CX and quantification is shown on the bar graph. Values represent the mean ± SEM of 3 independent experiments. Iba-1^{+} cells exhibit similar arborization in the CX of WT CPZ and *Lgals3*$^{-/-}$ CPZ mice. ns: non-significant; oneway analysis of variance (ANOVA) followed by Bonferroni post-hoc tests. C: Iba-1 and CD45 co-immunohistochemistry in CC. Microscopic studies were done in the area delineated by a dotted box (CC). Images from CC were obtained by confocal microscopy in the z axis and were reconstructed to obtain a 3D figure using Image J software (z-stack). D: Flow cytometry analysis of CD11b/CD45^{high} cells. CD11b^{+} were purified by magnetic microbeads conjugated to an antibody against CD11b, followed by immunostaining with a specific antibody against CD11-PE and CD45-FITC and evaluated by flow cytometry. Data were processed with Winmdi 2.8 Software. Pre-immune sera were used as negative controls for polyclonal antibodies.

for F4/80 (not shown), which is not expressed in lymphocytes. In addition, when Iba-1^{+}/CD45^{high} cells were evaluated by immunohistochemistry, only a few were found to be positive for both markers and no significant differences were observed between *Lgals3*$^{-/-}$ and WT mice (Figs. 7C and D), although this analysis does allow for a distinction between CD11b^{+}/CD45^{high} and CD11b^{+}/CD45^{high*}. To investigate whether the increased frequency of CD11b^{+}/CD45^{high} cells originates from monocytes, brain sections were stained after 5 weeks with Ly6C. No Ly6C^{+} cells were detected in either *Lgals3*$^{-/-}$ or WT mice (Supplementary Fig. 3), which suggests that the macrophages observed (CD11b^{+}/CD45^{+} cells) could not have originated from monocytes and that the migration of these cells was not induced by Gal-3 deficiency. Finally, mRNA was analyzed by RT-PCR for inflammatory molecules such as CCL2 and M-CSF in samples from CC and CX of WT or *Lgals3*$^{-/-}$ mice in the fifth week of CPZ-induced demyelination. While no significant differences were observed among the different groups analyzed for M-CSF, a significant increase was observed for CCL2 in CC *Lgals3*$^{-/-}$ mice (Fig. 9B).

Behavioral studies

The behavior of WT and *Lgals3*$^{-/-}$ mice after 2 and 5 weeks of CPZ treatment in the plus-maze, locomotor activity and Y-maze tests is shown in Fig. 8. After 2 weeks of CPZ treatment, both WT and *Lgals3*$^{-/-}$ mice increased significantly the percentage of open arm entries ($P < 0.05$ and $P < 0.001$, respectively); only CPZ-treated *Lgals3*$^{-/-}$ mice showed an augmented percentage of time spent in open arms ($P < 0.001$), while the number of total arm entries was not modified in the plus maze test (Fig. 10A). These results suggest that WT and *Lgals3*$^{-/-}$ mice have lower levels of innate anxiety than their naive counterparts after 2 weeks of CPZ treatment. Furthermore, *Lgals3*$^{-/-}$ mice treated with CPZ for 2 weeks also showed a significant decrease in the counts measured in the locomotor activity test ($P < 0.05$, Fig. 10B), which hints at diminished locomotor activity. Interestingly, 2-week exposure to CPZ lowered the percentage of spontaneous alternation of *Lgals3*$^{-/-}$ mice in the Y-maze test ($P < 0.05$, Fig. 10C) but produced no significant changes in the WT group. After 5 weeks of CPZ

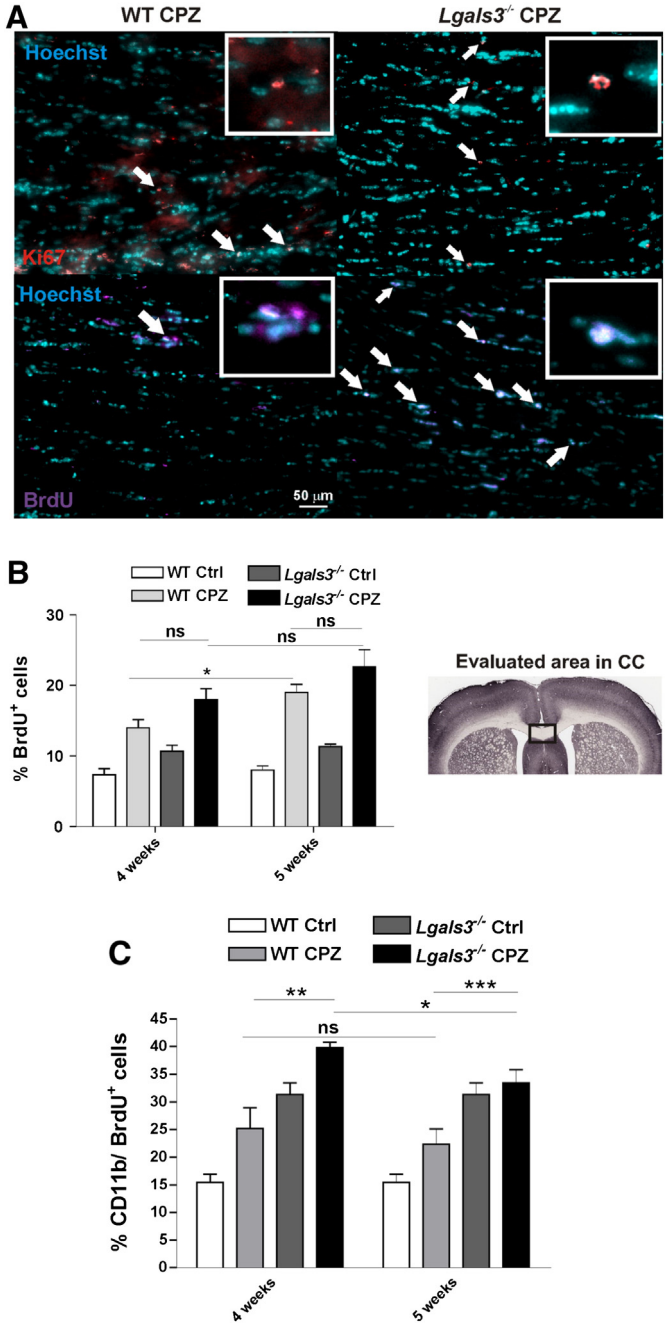

Fig. 8. Variations in cell proliferation and microglial phenotype during demyelination. A: Representative immunohistochemical staining of $Ki67^+$ (red) and $BrdU^+$ (violet) in CC sections at the fifth week of treatment. Nuclei were marked with Hoechst 33342. White boxes show insets of proliferating cells in each condition. Proliferating cells are indicated with white arrows. B: The graph shows the amount of $BrdU^+$ cells in the CC in both WT and *Lgals3*$^{-/-}$ animals fed with CPZ at 4 and 5 weeks of treatment. $BrdU^+$ cells were analyzed and quantified in the area of CC depicted by the box in the scheme. Cells were regarded as $BrdU^+$ positive only when co-localizing with Hoechst nuclear staining. C: Flow cytometry analysis of $BrdU^+$ cells in pre-sorted microglial cells ($CD11b^+$) from CC at the fifth week of treatment. $CD11b^+$ were purified by magnetic microbeads conjugated to an antibody against CD11b, followed by immunostaining with a specific anti-BrdU antibody and evaluated by flow cytometry. Data were processed with Winmdi 2.8 Software. Pre-immune sera were used as negative controls for polyclonal antibodies. Isotype controls were used for specific monoclonal antibodies. At least 6 mice per experimental condition in each time point were analyzed. Values are expressed as the mean ± SEM. Comparisons were performed using the ANOVA statistical test (ns: non significant; *$P < 0.05$; **$P < 0.01$; ***$P < 0.001$).

treatment, both WT and *Lgals3*$^{-/-}$ mice significantly decreased the number of total arm entries in the plus maze ($P < 0.05$; Fig. 10D) and the Y-maze tests ($P < 0.001$ and $P < 0.05$, respectively; Fig. 10F). There was also a remarkable reduction in locomotor activity counts in the locomotor activity test ($P < 0.001$ and $P < 0.01$; Fig. 10E). No other differences were found in the parameters measured either in the hole-board or the inverted screen tests (data not shown).

Discussion

Galectins, an evolutionarily conserved family of animal lectins, display multiple roles in diverse immune cell processes, shaping the course of adaptive immune responses and fine-tuning the inflammatory response (Rabinovich and Croci, 2012). In particular, Gal-3 is expressed by a variety of immune cells at the periphery during innate and adaptive immune response (Leffler et al., 2004; Rabinovich et al., 2007; Yang et al., 2008). Gal-3 is expressed and secreted by peripheral macrophages (Sato et al., 1993; Sato and Hughes, 1994) and its binding to different cell surface glycosylated receptors induces immune cell activation, differentiation and survival (Rabinovich and Croci, 2012). Both adaptive and innate immune responses are controlled by Gal-3. For example, through the formation of supramolecular networks—called lattices—with N-glycans on the T cell receptor (TCR), Gal-3 increases the threshold of antigen-driven T cell activation (Demetriou et al., 2001). While the role of Gal-3 is relatively well defined in peripheral immune cells, little is known about its role in the CNS. Gal-3 is upregulated in the spinal cord and optic nerves of mice with EAE (Reichert and Rotshenker, 1999), suggesting its potential role in modulating neuroimmune processes. In addition, Gal-3 stimulates neural cell adhesion and neurite growth (Pesheva et al., 1998), whereas it inhibits Schwann cell proliferation in cultured sciatic nerves (Gustavsson et al., 2007). Interestingly, in previous work we demonstrated that Gal-3 promotes OLG differentiation and contributes to myelin integrity and function (Pasquini et al., 2011). Moreover, Gal-3 is also involved in the modulation of cell motility in the rostral migratory stream (Comte et al., 2011).

Microglia, the only resident hematopoietic cells in the CNS, participate in the regulation of immune responses due to their phagocytic capacity and their ability to present antigens and secrete immunoregulatory mediators such as cytokines, growth factors and chemokines (Perry and Gordon, 1991). Whether microglia play a harmful or beneficial role during CNS inflammation has been extensively debated (Block et al., 2007; Hanisch and Kettenmann, 2007). Similar to the M1 and M2 phenotypes of peripheral macrophages (Gordon, 2003; Martinez et al., 2008; Mosser, 2003), microglia might fulfil both roles through different phenotypes with distinctive functions in the control of both degenerative and regenerative processes (Starossom et al., 2012). In this regard, remyelination often fails in multiple sclerosis (MS), leading to long term disability (Franklin, 2002). MS is characterized by acute demyelinating lesions with T cell infiltrates and activated macrophages (Adams et al., 1989; Hickey, 1999). However, OLG apoptosis occurs in both active and newly formed lesions even in the absence of these peripheral cells, which results in infiltration and activation of local microglia (Barnett and Prineas, 2004; Barnett et al., 2006; Gay, 2006; Henderson et al., 2009). Phagocytosis of myelin debris by microglia and macrophages plays an important role in the initiation of remyelination, as OPC differentiation can be inhibited by myelin (Kotter et al., 2006). Myelin phagocytosis is mediated by CR3/MAC-1 and SRAI/II, which are regulated by Gal-3-dependent activation of PI3K; as a consequence, myelin phagocytosis is deficient in *Lgals3*$^{-/-}$ microglia (Rotshenker et al., 2008). Our results show that the OPC generated in response to CPZ-induced demyelination in *Lgals3*$^{-/-}$ mice have decreased ability to differentiate, which could be due to the inhibitory effects exerted by impaired phagocytosis of myelin debris in *Lgals3*$^{-/-}$ microglia. Moreover, this could also be explained by recent findings demonstrating that conditioned media from Gal-3-expressing—but not *Lgals3*$^{-/-}$—microglia successfully promote OLG differentiation (Pasquini et al., 2011).

TREM-2b has recently been described as a central mediator of phagocytosis involved in debris clearance. The loss-of-function mutation of the microglial receptor TREM-2b leads to a rare hereditary

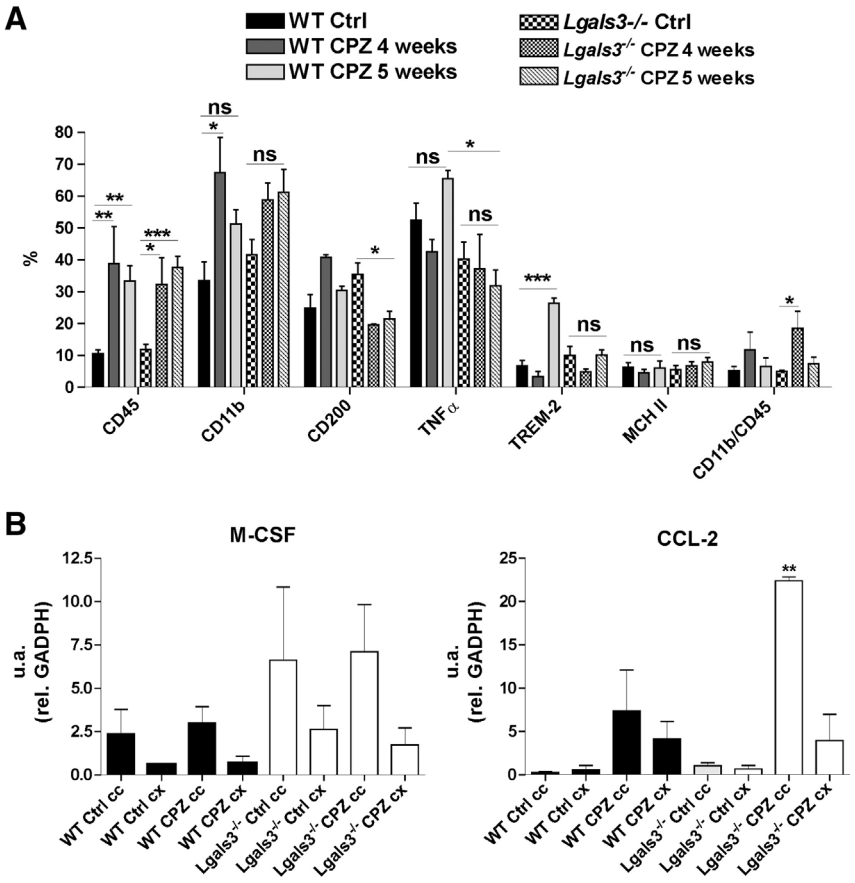

Fig. 9. A: Flow cytometry analysis of cell surface receptors and cytokine production by pre-sorted microglial cells ($CD11b^+$) from CC at the fifth week of treatment. $CD11b^+$ were purified by magnetic microbeads conjugated to an antibody against CD11b, followed by immunostaining with a specific antibody against cell surface receptors and cytokines and evaluated by flow cytometry. Data were processed with Winmdi 2.8 Software. Pre-immune sera were used as negative controls for polyclonal antibodies. Isotype controls were used for specific monoclonal antibodies. At least 6 mice per experimental condition in each time point were analyzed. Values are expressed as the mean ± SEM. Comparisons were performed using the ANOVA statistical test (ns: non significant; *P < 0.05; **P < 0.01; ***P < 0.001). B: Results of CCL2 (a) and M-CSF (b) gene expression analysis by RT-PCR of the entire CC or CX. Data are expressed relative to GAPDH mRNA (±SEM). Values were normalized against a housekeeping gene (GAPDH) and expressed relative to the respective control levels. Notice that only CCL2 mRNA expression levels in CC of CPZ-treated *Lgals3*$^{-/-}$ mice were significantly increased. Comparisons were performed using one way analysis of variance (ANOVA) followed by Bonferroni post-hoc tests (**P ≤ 0.01).

disease named polycystic lipomembranous osteodysplasia with sclerosing leukoencephalopathy (PLOSL), or Nasu–Hakola disease (Hakola, 1972; Nasu et al., 1973; Paloneva et al., 2001), which is characterized by a combination of progressive presenile dementia and sclerosing leukoencephalopathy with bone cysts and which is most likely caused by an impaired phagocytic function of microglia (Paloneva et al., 2002). Piccio et al. (2007) demonstrated that TREM-2b expression is upregulated in the spinal cord during the early, inflammatory and chronic phases of EAE in microglial cells, and that its blockade during the effector phase of EAE results in disease exacerbation. Moreover, the intravenous inoculation of TREM-2-transduced myeloid cells leads to the amelioration of EAE associated with increased myelin phagocytosis (Takahashi et al., 2007). A pronounced increase in microglial phagocytosis has been reported during CPZ-induced demyelination. This increase is associated with the upregulation of phagocytic receptors, including TNF-α production and early induction of CD200R, although TREM-2b plays the most prominent role (Voß et al., 2011). Interestingly, our results show that *Lgals3*$^{-/-}$ mice are unable to induce TREM-2b and increase TNF-α production. They also exhibit a significant decrease in CD200R as a response to CPZ intoxication, indicating that the absence of Gal-3 leads to altered microglial response to CPZ treatment.

Recently, Lalancette-Hébert et al. (2012) demonstrated that Gal-3 plays a pivotal role in mediating injury-induced microglial activation and proliferation using a unilateral transient focal cerebral ischemia model in mice. In accordance with these findings, our studies show the incapacity of Gal-3-deficient microglia to induce ED1 expression. On the other hand, in contrast with evidence provided by Lalancette-Hébert et al. in their model, our results display a higher proliferative response of microglia to CPZ-induced demyelination in *Lgals3*$^{-/-}$ relative to WT mice. In our experiments, although *Lgals3*$^{-/-}$ mice generated a higher number of cells with increased surface expression of CD11b, these cells did not express ED1 and evidenced higher caspase-3 activation. This effect could be linked to the well-established anti-apoptotic role of Gal-3 (Yang et al., 1996).

The CPZ-induced demyelination model in TNF-α-knockout mice showed a delay in remyelination associated with a reduction in OPC proliferation (Arnett et al., 2001). The regenerative effect of TNF-α in CPZ mice was mediated by the TNF receptor 2 (TNFR2) but not by TNFR1. This suggests a dual role for TNF-α in demyelination and remyelination, depending on the underlying signaling pathway. In TNF-α-knockout mice, remyelination was inhibited due to a delay in OPC differentiation into mature OLG (Mason et al., 2001b). Accordingly, our results show that *Lgals3*$^{-/-}$ mice do not increase TNF-α production in response to CPZ intoxication, which could also explain the decrease in OPC differentiation and the failure of *Lgals3*$^{-/-}$ mice to initiate spontaneous remyelination.

Previous studies reveal that CCL2 (MCP1) might be involved in MS pathology. Anti-CCL2 significantly reduces the severity of relapsing EAE (Karpus and Kennedy, 1997). Also, CCL2 mRNA levels have been observed to transiently increase in the first week of CPZ treatment and to return to control levels as from the second week of treatment, suggesting that CCL2 mediates early microglia activation. Comparative

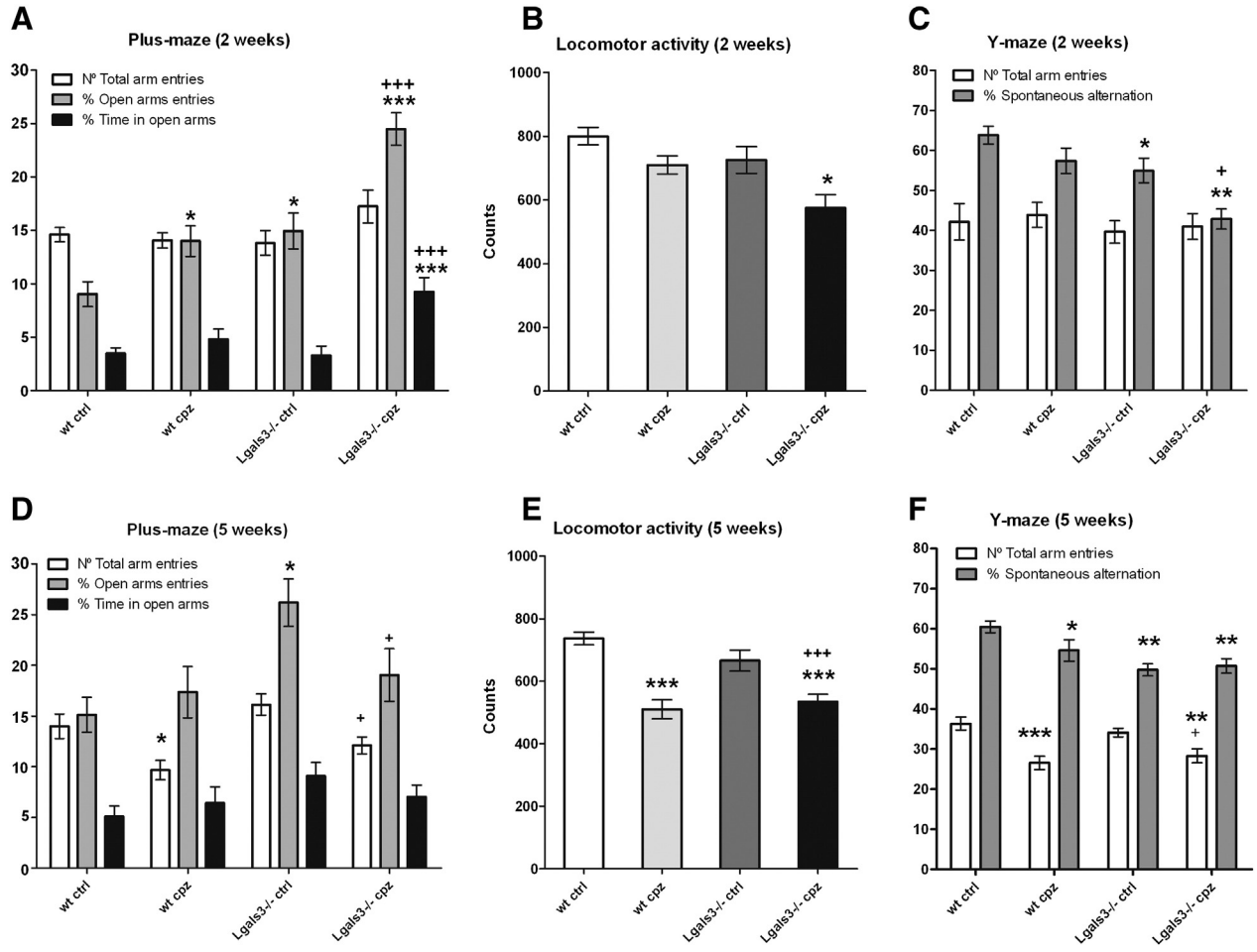

Fig. 10. Performance of WT and *Lgals3*$^{-/-}$ mice after 2 (A, B, C) and 5 (D, E, F) weeks of CPZ treatment in the plus-maze, locomotor activity and Y-maze tests. Results are expressed as the mean ± SEM of (A and D) total arm entries, percentage of open arm entries and percentage of time spent in open arms measured in the plus-maze test; (B and E) locomotor activity counts; and (C and F) total arm entries and percentage of spontaneous alternation measured in the Y-maze. *P < 0.05; **P < 0.01 and ***P < 0.001 significantly different from WT mice; $^{+}$P < 0.05 and $^{+++}$P < 0.001 significantly different from *Lgals3*$^{-/-}$ mice; Newman–Keuls Multiple Comparison Test after one way ANOVA.

analyses revealed that CCL2, at least at the mRNA level, was greater in the CC as compared to the CX region (Buschmann et al., 2012). Moreover, the polarization of M2 macrophages was associated with a decrease in inflammatory cytokine IL-1β, TNF-α and CCL2 (Liu et al., 2013). Remarkably, our results show that only CPZ-treated *Lgals3*$^{-/-}$ mice kept CCL2 mRNA levels significantly increased in the CC until the fifth week, suggesting that the absence of Gal-3 prevents the shift from M1 to M2 microglia.

Jiang et al. (2009) have demonstrated that *Lgals3*$^{-/-}$ mice exhibit sharply reduced macrophage infiltration in the CNS during EAE, which leads to reduced severity of the disease. These results supported the key role of Gal-3 in promoting inflammation via local recruitment of leukocytes. The CPZ model offers the opportunity to investigate CNS processes leading to remyelination independently of the contribution of the peripheral immune system, as there is no breakdown of the blood brain barrier (BBB). Distinct from EAE, CPZ-induced demyelination is characterized by the accumulation of resident microglia with very few peripheral macrophages (McMahon et al., 2002; Yagi et al., 2004). Moreover, CPZ-induced demyelination does not involve the accumulation of T cells, presumably because the BBB is not compromised (Bakker and Ludwin, 1987; Kondo et al., 1987).

The 21.5 kDa MBP isoform is the first of classic isoforms to be synthesized from OPC which promotes not only their proliferation but also enhances their branching (Smith et al., 2013). Whereas these roles are dependent on the subcellular localization of 21.5 kDa MBP to the nucleus, other MBP isoforms including 18.2 kDa and 14.0 kDa are localized closer to the membrane and are involved in myelin compacting and stabilization (Chernoff, 1981). Our data (Fig. 1E) show a dramatic decrease in 21.5 kDa MBP isoform even when Gal-3 is absent. Our results further show that these isoforms are affected by CPZ demyelination in the absence of Gal-3, suggesting that Gal-3 might modulate the stabilization or expression of these isoforms during CPZ demyelination, and might account for the lack of myelin observed in *Lgals3*$^{-/-}$ mice. Additionally, Gal-3 seems to play a role at the early stages of OPC maturation, as a decrease in the branching of the arborization processes is evident in its absence (Fig. 2). One possibility is that Gal-3 might act intracellularly by regulating both the subcellular localization of 21.5 kDa MBP isoform and the expression and/or stabilization of the 18.5 kDa and 14.0 kDa isoforms. On the other hand, Gal-3 could function extracellularly by reacting to different glycosylated molecules such as CSPG (NG2^{+} cells), thus inducing OPC maturation.

The analysis of axon caliber distribution has been used to describe developmental myelination processes as well as states of active remyelination. A significant reduction in the mean value for axonal diameter has been previously described during acute demyelination (Mason et al., 2001a). One of the possibilities could be a degeneration process of large axons, while another explanation might be a functional relationship between axons and myelin which alters axonal caliber. Our results show a significant reduction in axonal caliber in *Lgals3*$^{-/-}$ mice, reflecting their basal demyelination. CPZ demyelination in these

animals led to a loss of small axons, an effect probably due to basal demyelination, which promoted their degeneration under induced demyelination.

Animal behavior, which reflects the interaction of diverse individual factors, is often used as a means to study the in vivo function of different biological systems. Mice treated with CPZ exhibit weight loss and developed both motor and behavioral deficiencies (Franco-Pons et al., 2007; Xu et al., 2009). In addition, behavioral changes in rodents upon long-term CPZ exposure may be reminiscent of psychiatric disorders (Gregg et al., 2009; Xu et al., 2009). Some of these signs and symptoms have been successfully ameliorated by neuroleptic treatment (Xu et al., 2010, 2011; Zhang et al., 2008), suggesting that long-term exposure to CPZ may recapitulate psychiatric manifestations associated with MS and related conditions involving white matter damage. In this regard, we have previously demonstrated that *Lgals3*$^{-/-}$ mice have decreased anxiety behavior, similar to that observed in the early demyelination process following CPZ intoxication (Pasquini et al., 2011). Interestingly, hypertensive rats, which serve as a spontaneous model of attention deficit hyperactivity, show behavior deficits, appearing considerably more active and showing less anxiety-related behavior and memory impairment. Surprisingly, these hypertensive rats have demonstrated a lower expression of Gal-3 in brain prefrontal CX, and miRNA microarray screening has proven that rno-let-7d, which has a binding site at Gal-3 mRNA, was considerably upregulated (Wu et al., 2010). Accordingly, the lack of Gal-3 and altered myelin structure in *Lgals3*$^{-/-}$ mice has led to behavioral abnormalities including lower levels of anxiety and impairment of the spatial working memory. CPZ effects on behavior are observed earlier in *Lgals3*$^{-/-}$ mice, which is likely due to the early depletion of their mature OLG pool, as CPZ treatment induces mature OLG apoptosis as early as a few days after the initiation of the CPZ diet and weeks before demyelination is evident (Buschmann et al., 2012; Hesse et al., 2010).

In summary, we demonstrate here that Gal-3 is upregulated in microglial cells during CPZ-induced demyelination and acts as an important modulator of microglial activation and phenotype, driving the onset of remyelination. We report that Gal-3 deficiency leads to (1) a similar susceptibility to CPZ-induced demyelination but an inability to initiate spontaneous remyelination, (2) a decrease in the differentiation of OPC, (3) a defective microglial activation during demyelination, associated with a significant increase in the number of proliferating microglial cells with higher levels of CD11b and caspase-3 activation but without ED1 expression, (4) a failure of microglial cells to induce TREM-2b expression or to produce TNF-α, and (5) early behavioral alterations including lower levels of anxiety, decreased locomotor activity and impairment of the spatial working memory.

A recently published work has demonstrated that OLG differentiation is enhanced in vitro with M2 cell conditioned media and impaired in vivo following intra-lesional M2 cell depletion. Moreover, M2 cell polarization is essential for efficient remyelination (Miron et al., 2013). Therefore, Gal-3, expressed in microglial cells, could favor the onset of remyelination through the induction of M2 cell polarization or a direct effect on OLG differentiation, either extra or intracellularly. Our results may have important implications in the development of future therapies for a variety of demyelinating diseases such as MS.

Supplementary data to this article can be found online at http://dx.doi.org/10.1016/j.nbd.2013.10.023.

Acknowledgments

We thank Fu-Tong Liu for kindly providing *Lgals3*$^{-/-}$ mice. Dr. J. Correale for support in discussion. We also thank Daniela B. Ureta for excellent assistance in flow cytometry and Marianela Vence for dedicated mice care. This study was supported by grants from the Argentinean Agency for Promotion of Science and Technology (PICT 2006-2368 and PICT 2008-0791 to J.M.P. and PICT 2008-1182 to L.A.P.), grants from the University of Buenos Aires (UBACYT-20020100100393 to L.A.P., CONICET PIP-112-200801-01767 to L.A.P. and J.M.P.), and grants from the National Multiple Sclerosis Society (NMSS) (RG4530 to G.A.R.), Argentinean Agency for Promotion of Science and Technology (PICT 2010-870 to G.A.R.) and Fundación Sales (to G.A.R.).

References

Adams, C.W., Poston, R.N., Buk, S.J., 1989. Pathology, histochemistry and immunocytochemistry of lesions in acute multiple sclerosis. J. Neurol. Sci. 92, 291–306.
Arnett, H.A., Mason, J., Marino, M., Suzuki, K., Matsushima, G.K., Ting, J.P., 2001. TNF alpha promotes proliferation of oligodendrocyte progenitors and remyelination. Nat. Neurosci. 4, 1116–1122.
Bakker, D.A., Ludwin, S.K., 1987. Blood–brain barrier permeability during cuprizone-induced demyelination. Implications for the pathogenesis of immune-mediated demyelinating diseases. J. Neurol. Sci. 78, 125–137.
Barnett, M.H., Prineas, J.W., 2004. Relapsing and remitting multiple sclerosis: pathology of the newly forming lesion. Ann. Neurol. 55, 458–468.
Barnett, M.H., Henderson, A.P., Prineas, J.W., 2006. The macrophage in MS: just a scavenger after all? Pathology and pathogenesis of the acute MS lesion. Mult. Scler. 12, 121–132.
Blakemore, W.F., 1973. Demyelination of the superior cerebellar peduncle in the mouse induced by cuprizone. J. Neurol. Sci. 20 (1), 63–72.
Block, M.L., Zecca, L., Hong, J.S., 2007. Microglia-mediated neurotoxicity: uncovering the molecular mechanisms. Nat. Rev. Neurosci. 8, 57–69.
Buschmann, J.P., Berger, K., Awad, H., Clarner, T., Beyer, C., Kipp, M., 2012. Inflammatory response and chemokine expression in the white matter corpus callosum and gray matter cortex region during cuprizone-induced demyelination. J. Mol. Neurosci. 48 (1), 66–76.
Chernoff, G.F., 1981. Shiverer: an autosomal recessive mutant mouse with myelin deficiency. J. Hered. 72 (2), 128.
Comte, I., Kim, Y., Young, C.C., van der Harg, J.M., Hockberger, P., Bolam, P.J., Poirier, F., Szele, F.G., 2011. Galectin-3 maintains cell motility from the subventricular zone to the olfactory bulb. J. Cell Sci. 124 (14), 2438–2447.
Coughenour, L.L., McLean, J.R., Parker, R.B., 1977. A new device for the rapid measurement of impaired motor function in mice. Pharmacol. Biochem. Behav. 6 (3), 351–353.
Dellu, F., Contarino, A., Simon, H., Koob, G.F., Gold, L.H., 2000. Genetic differences in response to novelty and spatial memory using a two-trial recognition task in mice. Neurobiol. Learn. Mem. 73 (1), 31–48.
Demetriou, M., Granovsky, M., Quaggin, S., Dennis, J.W., 2001. Negative regulation of T-cell activation and autoimmunity by Mgat5 N-glycosylation. Nature 409 (6821), 733–739.
Fernández, S.P., Wasowski, C., Loscalzo, L.M., Granger, R.E., Johnston, G.A., Paladini, A.C., Marder, M., 2006. Central nervous system depressant action of flavonoid glycosides. Eur. J. Pharmacol. 539, 168–176.
Ford, A.L., Goodsall, A.L., Hickey, W.F., Sedgwick, J.D., 1995. Normal adult ramified microglia separated from other central nervous system macrophages by flow cytometric sorting. Phenotypic differences defined and direct ex vivo antigen presentation to myelin basic protein-reactive CD4+ T cells compared. J. Immunol. 154, 4309–4321.
Franco-Pons, N., Torrente, M., Colomina, M.T., Vilella, E., 2007. Behavioral deficits in the cuprizone-induced murine model of demyelination/remyelination. Toxicol. Lett. 169 (3), 205–213 (30).
Franklin, R.J., 2002. Why does remyelination fail in multiple sclerosis? Nat. Rev. Neurosci. 3, 705–714.
Gay, F.W., 2006. Early cellular events in multiple sclerosis. Intimations of an extrinsic myelinolytic antigen. Clin. Neurol. Neurosurg. 108, 234–240.
Gordon, S., 2003. Alternative activation of macrophages. Nat. Rev. Immunol. 3, 23–35.
Gregg, J.R., Herring, N.R., Naydenov, A.V., Hanlin, R.P., Konradi, C., 2009. Downregulation of oligodendrocyte transcripts is associated with impaired prefrontal cortex function in rats. Schizophr. Res. 113, 277–287.
Gustavsson, P., Linsmeier, C.E., Leffler, H., Kanje, M., 2007. Galectin-3 inhibits Schwann cell proliferation in cultured sciatic nerve. Neuroreport 18, 669–673.
Hakola, H.P., 1972. Neuropsychiatric and genetic aspects of a new hereditary disease characterized by progressive dementia and lipomembranous polycystic osteodysplasia. Acta Psychiatr. Scand. Suppl. 232, 1–173.
Hanisch, U.K., Kettenmann, H., 2007. Microglia: active sensor and versatile effector cells in the normal and pathologic brain. Nat. Neurosci. 10, 1387–1394.
Henderson, A.P., Barnett, M.H., Parratt, J.D., Prineas, J.W., 2009. Multiple sclerosis: distribution of inflammatory cells in newly forming lesions. Ann. Neurol. 66, 739–753.
Hesse, A., Wagner, M., Held, J., Bruck, W., Salinas-Riester, G., Hao, Z., et al., 2010. In toxic demyelination oligodendroglial cell death occurs early and is FAS independent. Neurobiol. Dis. 37 (2), 362–369.
Hickey, W.F., 1999. The pathology of multiple sclerosis: a historical perspective. J. Neuroimmunol. 98, 37–44.
Hiremath, M.M., Saito, Y., Knapp, G.W., Ting, J.P., Suzuki, K., Matsushima, G.K., 1998. Microglial/macrophage accumulation during cuprizone-induced demyelination in C57BL/6 mice. J. Neuroimmunol. 92 (1–2), 38–49.
Hsu, D.K., Yang, R.Y., Pan, Z., Yu, L., Salomon, D.R., Fung-Leung, W.P., et al., 2000. Targeted disruption of the Galectin-3 gene results in attenuated peritoneal inflammatory responses. Am. J. Pathol. 156 (3), 1073–1083.
Jiang, H.R., Al Rasebi, Z., Mensah-Brown, E., Shahin, A., Xu, D., Goodyear, C.S., et al., 2009. Galectin-3 deficiency reduces the severity of experimental autoimmune encephalomyelitis. J. Immunol. 182, 1167–1173.
Karpus, W.J., Kennedy, K.J., 1997. MIP-1alpha and MCP-1 differentially regulate acute and relapsing autoimmune encephalomyelitis as well as Th1/Th2 lymphocyte differentiation. J. Leukoc. Biol. 62 (5), 681–687.

Kondo, A., Nakano, T., Suzuki, K., 1987. Blood–brain barrier permeability to horseradish peroxidase in twitcher and cuprizone-intoxicated mice. Brain Res. 425, 186–190.
Kotter, M.R., Li, W.W., Zhao, C., Franklin, R.J., 2006. Myelin impairs CNS remyelination by inhibiting oligodendrocyte precursor cell differentiation. J. Neurosci. 26, 328–332.
Lalancette-Hébert, M., Gowing, G., Simard, A., Weng, Y.C., Kriz, J., 2007. Selective ablation of proliferating microglial cells exacerbates ischemic injury in the brain. J. Neurosci. 27, 2596–2605.
Lalancette-Hébert, M., Swarup, V., Beaulieu, J.M., Bohacek, I., Abdelhamid, E., Weng, Y.C., et al., 2012. Galectin-3 is required for resident microglia activation and proliferation in response to ischemic injury. J. Neurosci. 32 (30), 10383–10395.
Langrish, C.L., Chen, Y., Blumenschein, W.M., Mattson, J., Basham, B., Sedgwick, J.D., et al., 2005. IL-23 drives a pathogenic T cell population that induces autoimmune inflammation. J. Exp. Med. 201 (2), 233–240.
Leffler, H., Carlsson, S., Hedlund, M., Qian, Y., Poirier, F., 2004. Introduction to galectins. Glycoconj. J. 19 (7–9), 433–440.
Lein, E.S., Hawrylycz, M.J., Ao, N., Ayres, M., Bensinger, A., Bernard, A., et al., 2007. Genome-wide atlas of gene expression in the adult mouse brain. Nature 445, 168–176.
Li, Y., Komai-Koma, M., Gilchrist, D.S., Hsu, D.K., Liu, F.T., Springall, T., et al., 2008. Galectin-3 is a negative regulator of lipopolysaccharide-mediated inflammation. J. Immunol. 181 (4), 2781–2789.
Lister, R.G., 1987. The use of a plus maze to measure anxiety in the mouse. Psychopharmacology (Berl) 92, 180–185.
Liu, C., Li, Y., Yu, J., Feng, L., Hou, S., Liu, Y., et al., 2013. Targeting the shift from M1 to M2 macrophages in experimental autoimmune encephalomyelitis mice treated with fasudil. PLoS One 8 (2), e54841.
Ludwin, S.K., 1978. Central nervous system demyelination and remyelination in the mouse: an ultrastructural study of cuprizone toxicity. Lab. Invest. 39, 597–612.
Martinez, F.O., Sica, A., Mantovani, A., Locati, M., 2008. Macrophage activation and polarization. Front. Biosci. 13, 453–461.
Mason, J.L., Suzuki, K., Chaplin, D.D., Matsushima, G.K., 2001a. Interleukin-1beta promotes repair of the CNS. J. Neurosci. 21, 7046–7052.
Mason, J.L., Langaman, C., Morell, P., Suzuki, K., Matsushima, G.K., 2001b. Episodic demyelination and subsequent remyelination within the murine central nervous system: changes inaxonal calibre. Neuropathol. Appl. Neurobiol. 27 (1), 50–58.
Matsushima, G.K., Morell, P., 2001. The neurotoxicant, cuprizone, as a model to study demyelination and remyelination in the central nervous system. Brain Pathol. 11, 107–116.
McMahon, E.J., Suzuki, K., Matsushima, G.K., 2002. Peripheral macrophage recruitment in cuprizone-induced CNS demyelination despite an intact blood–brain barrier. J. Neuroimmunol. 130, 32–45.
Miron, V.E., Boyd, A., Zhao, J.W., Yuen, T.J., Ruckh, J.M., Shadrach, J.L., et al., 2013. M2 microglia and macrophages drive oligodendrocyte differentiation during CNS remyelination. Nat. Neurosci. 16 (9), 1211–1218.
Mok, S.W., Thelen, K.M., Riemer, C., Bamme, T., Gültner, S., Lütjohann, D., et al., 2006. Simvastatin prolongs survival times in prion infections of the central nervous system. Biochem. Biophys. Res. Commun. 348 (2), 697–702.
Mok, S.W., Riemer, C., Madela, K., Hsu, D.K., Liu, F.T., Gültner, S., et al., 2007. Role of galectin-3 in prion infections of the CNS. Biochem. Biophys. Res. Commun. 359 (3), 672–678.
Morell, P., Barrett, C.V., Mason, J.L., Toews, A.D., Hostettler, J.D., Knapp, G.W., et al., 1998. Gene expression in brain during cuprizone-induced demyelination and remyelination. Mol. Cell. Neurosci. 12 (4–5), 220–227.
Mosser, D.M., 2003. Themany faces ofmacrophage activation. J. Leukoc. Biol. 73, 209–212.
Mouse Brain Library, 2003. A Human Brain Project, supported by the National Institue for Health (United States) and its institutes for Mental Health (NIMH), on Drug Abuse (NIDA) and on Alcohol Abuse and Alcoholism (NIAAA). www.mbl.org (on line version) .
Nasu, T., Tsukahara, Y., Terayama, K., 1973. A lipid metabolic disease–"membranous lipodystrophy"—an autopsy case demonstrating numerous peculiar membrane-structures composed of compound lipid in bone and bone marrow and various adipose tissues. Acta Pathol. 23, 539–558.
Nieminen, J., St-Pierre, C., Sato, S., 2005. Galectin-3 interacts with naive and primed neutrophils, inducing innate immune responses. J. Leukoc. Biol. 78, 1127–1135.
Olah, M., Amor, S., Brouwer, N., Vinet, J., Eggen, B., Biber, K., et al., 2012. Identification of a microglia phenotype supportive of remyelination. Glia 60 (2), 306–321.
Paloneva, J., Autti, T., Raininko, R., Partanen, J., Salonen, O., Puranen, M., et al., 2001. CNS manifestations of Nasu–Hakola disease: a frontal dementia with bone cysts. Neurology 56, 1552–1558.
Paloneva, J., Manninen, T., Christman, G., Hovanes, K., Mandelin, J., Adolfsson, R., et al., 2002. Mutations in two genes encoding different subunits of a receptor signaling complex result in an identical disease phenotype. Am. J. Hum. Genet. 71, 656–662.
Park, J.B., Yiu, G., Kaneko, S., Wang, J., Chang, J., He, X.L., et al., 2005. A TNF receptor family member, TROY, is a coreceptor with Nogo receptor in mediating the inhibitory activity of myelin inhibitors. Neuron 45 (3), 345–351.
Pasquini, L.A., Calatayud, C.A., Bertone Uña, A.L., Millet, V., Pasquini, J.M., Soto, E.F., 2007. The neurotoxic effect of cuprizone on oligodendrocytes depends on the presence of pro-inflammatory cytokines secreted by microglia. Neurochem. Res. 32 (2), 279–292.
Pasquini, L.A., Millet, V., Hoyos, H.C., Giannoni, J.P., Croci, D.O., Marder, M., et al., 2011. Galectin-3 drives oligodendrocyte differentiation to control myelin integrity and function. Cell Death Differ. 18, 1746–1756.
Perry, V.H., Gordon, S., 1991. Macrophages and the nervous system. Int. Rev. Cytol. 125, 203–244.
Pesheva, P., Kuklinski, S., Schmitz, B., Probstmeier, R., 1998. Galectin-3 promotes neural cell adhesion and neurite growth. J. Neurosci. Res. 54, 639–654.
Piccio, L., Buonsanti, C., Mariani, M., Cella, M., Gilfillan, S., Cross, A.H., et al., 2007. Blockade of TREM-2 exacerbates experimental autoimmune encephalomyelitis. Eur. J. Immunol. 37, 1290–1301.
Quinta, H.R., Galigniana, M.D., 2012. The neuroregenerative mechanism mediated by the Hsp90-binding immunophilin FKBP52 resembles the early steps of neuronal differentiation. Br. J. Pharmacol. 166, 637–649.
Rabinovich, G.A., Croci, D.O., 2012. Regulatory circuits mediated by lectin–glycan interactions in autoimmunity and cancer. Immunity 36, 322–335.
Rabinovich, G.A., Toscano, M.A., Jackson, S.S., Vasta, G.R., 2007. Functions of cell surface galectin–glycoprotein lattices. Curr. Opin. Struct. Biol. 17, 513–520.
Reichert, F., Rotshenker, S., 1999. Galectin-3/MAC-2 in experimental allergic encephalomyelitis. Exp. Neurol. 160 (2), 08–514.
Riemer, C., Neidhold, S., Burwinkel, M., Schwarz, A., Schultz, J., Krätzschmar, J., et al., 2004. Gene expression profiling of scrapie-infected brain tissue. Biochem. Biophys. Res. Commun. 323 (2), 556–564.
Rotshenker, S., 2009. The role of Galectin-3/MAC-2 in the activation of the innate-immune function of phagocytosis in microglia in injury and disease. J. Mol. Neurosci. 39, 99–103.
Rotshenker, S., Reichert, F., Gitik, M., Haklai, R., Elad-Sfadia, G., Kloog, Y., 2008. Galectin-3/MAC-2, Ras and PI3K activate complement receptor-3 and scavenger receptor-AI/II mediated myelin phagocytosis in microglia. Glia 56, 1607–1613.
Sato, S., Hughes, R.C., 1994. Regulation of secretion and surface expression of Mac-2, a galactoside-binding protein of macrophages. J. Biol. Chem. 269 (6), 4424–4430.
Sato, S., Nieminen, J., 2004. Seeing strangers or announcing "danger": galectin-3 in two models of innate immunity. Glycoconj. J. 19, 583–591.
Sato, S., Burdett, I., Hughes, R.C., 1993. Secretion of the baby hamster kidney 30-kDa galactose-binding lectin from polarized and nonpolarized cells: a pathway independent of the endoplasmic reticulum-Golgi complex. Exp. Cell Res. 207 (1), 8–18.
Sato, S., Ouellet, N., Pelletier, I., Simard, M., Rancourt, A., Bergeron, M.G., 2002. Role of galectin-3 as an adhesion molecule for neutrophil extravasation during streptococcal pneumonia. J. Immunol. 168, 1813–1822.
Sedgwick, J.D., Schwender, S., Imrich, H., Dorries, R., Butcher, G.W., ter Meulen, V., 1991. Isolation and direct characterization of resident microglial cells from the normal and inflamed central nervous system. Proc. Natl. Acad. Sci. U. S. A. 88, 7438–7442.
Smith, G.S., Samborska, B., Hawley, S.P., Klaiman, J.M., Gillis, T.E., Jones, N., et al., 2013. Nucleus-localized 21.5-kDa myelin basic protein promotes oligodendrocyte proliferation and enhances neurite outgrowth in coculture, unlike the plasma membrane-associated 18.5-kDa isoform. J. Neurosci. Res. 91, 349–362.
Starossom, S.C., Mascanfroni, I.D., Imitola, J., Cao, L., Raddassi, K., Hernandez, S.F., et al., 2012. Galectin-1 deactivates classically activated microglia and protects from inflammation-induced neurodegeneration. Immunity 37, 249–263.
Suzuki, K., Kikkawa, Y., 1969. Status spongiosus of CNS and hepatic changes induced by cuprizone (biscyclohexanone oxalyldihydrazone). Am. J. Pathol. 54, 307–325.
Takahashi, K., Prinz, M., Stagi, M., Chechneva, O., Neumann, H., 2007. TREM2- transduced myeloid precursors mediate nervous tissue debris clearance and facilitate recovery in an animal model of multiple sclerosis. PLoS Med. 4, e124.
Voß, E.V., Škuljec, J., Gudi, V., Skripuletz, T., Pul, R., Trebst, C., et al., 2011. Characterisation of microglia during de- and remyelination: can they create a repair promoting environment? Neurobiol. Dis. 45 (1), 519–528.
Weiner, H.L., 2008. A shift from adaptive to innate immunity: a potential mechanism of disease progression in multiple sclerosis. J. Neurol. 255 (1), 3–11.
Wu, L., Zhao, Q., Zhu, X., Peng, M., Jia, C., Wu, W., et al., 2010. A novel function of microRNA let-7d in regulation of galectin-3 expression in attention deficit hyperactivity disorder rat brain. Brain Pathol. 20, 1042–1054.
Xu, H., Yang, H.J., Zhang, Y., Clough, R., Browning, R., Li, X.M., 2009. Behavioral and neurobiological changes in C57BL/6 mice exposed to cuprizone. Behav. Neurosci. 123 (2), 418–429.
Xu, H., Yang, H.J., McConomy, B., Browning, R., Li, X.M., 2010. Behavioral and neurobiological changes in C57BL/6 mouse exposed to cuprizone: effects of antipsychotics. Front. Behav. Neurosci. 4, 8.
Xu, H., Yang, H.J., Rose, G.M., Li, X.M., 2011. Recovery of behavioral changes and compromised white matter in C57BL/6 mice exposed to cuprizone: effects of antipsychotic drugs. Front. Behav. Neurosci. 5, 31.
Yagi, T., Matsuda, J., Takikita, S., Mohri, I., Suzuki, K., Suzuki, K., 2004. Comparative clinicopathological study of saposin-A-deficient (SAP-A−/−) and Twitcher mice. J. Neuropathol. Exp. Neurol. 63 (7), 721–734.
Yang, L.J., Zeller, C.B., Shaper, N.L., Kiso, M., Hasegawa, A., Shapiro, R.E., et al., 1996. Gangliosides are neuronal ligands for myelin-associated glycoprotein. Proc. Natl. Acad. Sci. U. S. A. 93 (2), 814–818.
Yang, Z., Tsai, M.S., Wu, J.H., Herp, A., Wu, A.M., 2008. Defining the carbohydrate specificities of Erythrina corallodendron lectin (ECorL) as polyvalent Galbeta1-4GlcNAc (II) > monomeric II > monomeric Gal and GalNAc. Chang Gung Med. J. 31 (1), 26–43.
Zhang, Y., Xu, H., Jiang, W., Xiao, L., Yan, B., He, J., Wang, Y., et al., 2008. Quetiapine alleviates the cuprizone-induced white matter pathology in the brain of C57BL/6 mouse. Schizophr. Res. 106, 182–191.